Geochimica et Cosmochimica Acta 420 (2026) 131–147

Contents lists available at ScienceDirect

Geochimica et Cosmochimica Acta

journal homepage: www.elsevier.com/locate/gca

The effects of magmatic recharge on primary lunar melt compositions: Implications for the water and other volatile budget of the Moon

Dian Ji, Rajdeep Dasgupta, Cin-Ty Lee

Department of Earth, Environmental and Planetary Sciences, Rice University, Houston, TX 77005, United States of America

ARTICLE INFO

Associate editor: Shichun Huang

Keywords:
Moon
Lunar volatiles
Water
H_2O/Ce
Magmatic recharge

ABSTRACT

The theory of the Moon's formation via a giant impact, along with initial early sample analyses, suggested that the Moon is extremely volatile-depleted relative to the Earth. Yet, the petrologic studies of lunar melt inclusions and volcanic glasses over the last two decades suggested that water content in the lunar mantle is much higher (as high as 133 – 292 μg/g) than expected and is similar to the Earth's shallow upper mantle. This high water concentration of the lunar mantle challenged prevailing models of the formation and early evolution history of the Moon, suggesting that not all volatiles were lost, or that impactors supplied additional volatiles. However, previous petrologic models of lunar primary melt water content reconstruction did not consider many key magma differentiation processes. Here, we model lunar magmatism taking into consideration the process of magmatic recharge and show that such a process can explain the anomalously high water abundances, along with other volatile elements such as S, F, and Cl, in Apollo sample 74220 basaltic melt inclusions, as well as the available volatile data of Apollo 79135 and 15597 basaltic to andesitic melt inclusions. Moreover, the model can also explain the MgO content and high-Ti nature of 74220 inclusions, since recharge results in ever-increasing incompatible element concentrations while buffering major element compositions. Therefore, other than deriving from a wet background mantle, we propose an alternative scenario that the water-rich lunar melts could originate from a water-poor (as low as 1–22 μg/g), primitive, magma ocean cumulate. The estimated extent of volatile depletion of the lunar interior varies with the vigor of the magmatic recharge process. Further studies are necessary to independently assess evidence of magmatic recharge, the melt replenishment frequency, and the impact of such a magma reservoir process in our understanding of lunar mantle-crust evolution.

1. Introduction

The bulk silicate Moon has long been considered depleted in volatile elements compared to the bulk silicate Earth (Ringwood and Kesson, 1977; Taylor et al., 2006). This volatile depletion is consistent with the giant impact theory for the origin of the Moon (Cameron and Ward, 1976; Canup and Asphaug, 2001; Hartmann and Davis, 1975) as the large energy associated with the impact should have evaporated the volatiles, and may have been accompanied by subsequent incomplete accretion in the proto-lunar disk (Canup et al., 2015) and lunar magma ocean degassing (Day et al., 2007). This volatile element depletion on the Moon relative to the Earth is also supported by the isotopic studies of moderately volatile elements (e.g., Day and Moynier, 2014; Kato et al., 2015; Sharp et al., 2010). Determining lunar volatile abundance, however, is challenging, as there is no direct way to measure the composition of the lunar mantle. Using returned samples and lunar meteorites, attempts to reconstruct lunar mantle volatile budgets have focused on analyzing quenched melts (e.g., volcanic glass; Saal et al., 2008) or magma crystallization products (e.g., bulk rock mare basalt, apatite, and nominally anhydrous minerals; Barnes et al., 2014; Greenwood et al., 2011; Hui et al., 2013; Mallik et al., 2022; McCubbin et al., 2015; Pernet-Fisher et al., 2014; Robinson and Taylor, 2014; Tartèse et al., 2013). However, estimated water contents using these different methods vary by five orders of magnitude (Table S1), mainly due to uncertainties in extrapolating measured H contents to primary H contents or the actual meaning of measured H contents. For example, H in mare basalts can include a component from solar wind implantation or spallation reactions (Haskin and Warren, 1991), which needs to be considered and corrected accordingly. Volcanic glasses lose water during degassing, requiring extrapolation to reconstruct pre-degassed H contents. Using nominally anhydrous minerals to reconstruct pre-degassed melt H contents relies on H partition coefficients. However, uncertainties in these values are probably not well constrained. Accessory minerals, such as apatite, which incorporate H directly into their structure, can potentially

E-mail address: dj56@rice.edu (D. Ji).

https://doi.org/10.1016/j.gca.2026.03.042
Received 4 September 2025; Accepted 24 March 2026
Available online 28 March 2026

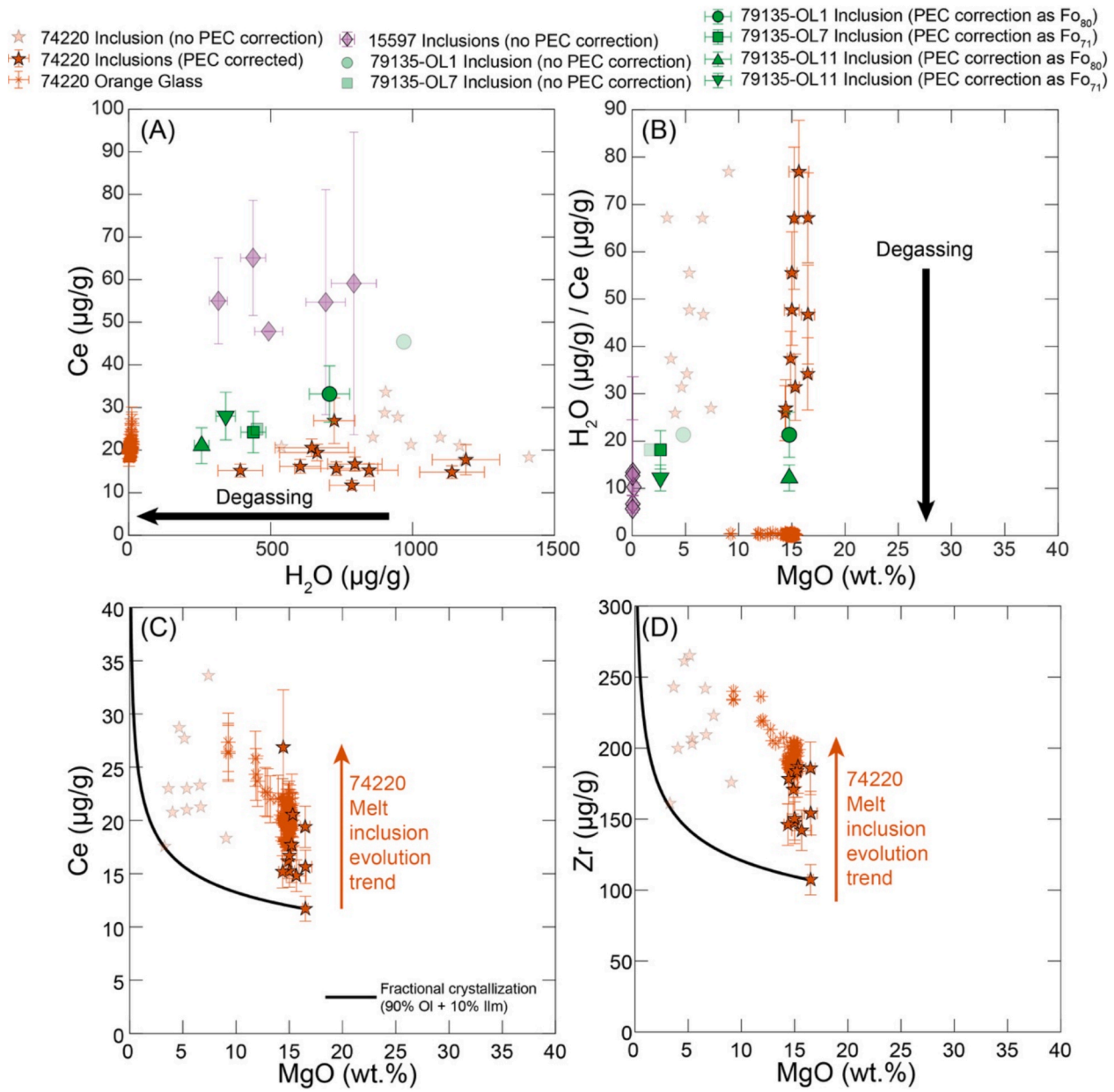

Fig. 1. (A) Concentrations of Ce versus H_2O and (B) H_2O/Ce versus MgO for melt inclusions in Apollo 74220, 79135, and 15597 samples, along with the orange glasses in 74220 for comparison. (C) Concentration of Ce versus MgO and (D) Zr versus MgO for melt inclusion and orange glasses in 74220. The semitransparent symbols represent the compositions of inclusions before the post-entrapment crystallization (PEC) correction. Different green symbols for the 79135-OL11-2 melt inclusions reflect different PEC correction assuming Fo71 and Fo80. The fractional crystallization calculation (Black solid line), assuming crystallized minerals consist of 90% of olivine and 10% of ilmenite, is estimated based on the modal percentages of phases reported by McIntosh et al., (2024) for crystallized 74220 glass beads. The partition coefficients of MgO, Ce, and Zr for olivine-melt and ilmenite-melt pairs are obtained from measurement on lunar olivine-bearing melt inclusion (Chen et al., 2022) and lunar relevant partitioning experiments (Dygert et al., 2013). The evolution trend of the 74220 melt inclusion cannot be explained solely by fractional crystallization.

preserve pre-degassing signatures (e.g., Boyce et al., 2010; Ji and Dygert, 2024). Still, such minerals are late-forming and do not record early magmatic states (Stephant et al., 2020). Importantly, even if pre-degassed signatures are obtained, extrapolating melt compositions to the mantle source requires correcting for the effects of magmatic differentiation and mantle melting conditions (e.g., Ji and Dasgupta, 2025). These processes are seldom well-constrained or critically considered.

The recent developments in in situ analysis of melt inclusions hold promise in resolving some of the above limitations, particularly the effects of degassing. Melt inclusions are trapped within phenocrysts, and have the potential to preserve the primitive melt composition. However, several syn- and post-entrapment processes may alter the original signatures of trapped melts. Some inclusions undergo post-entrapment crystallization or bubble formation; such a process can be reversed by the lab homogenization experiments or model calculations (Ni et al., 2017; Wallace et al., 2015). The trapped melt may also undergo syn-entrapment modification, where the compositions of inclusions deviate from the primitive melt because of the incorporation from the diffusive boundary layer (Audétat and Lowenstern, 2013), as well as some post-entrapment processes, such as decrepitation (Lowenstern, 1995; Zhang, 2024) and diffusion exchange between outer melt and the host mineral (Chen et al., 2013; Lloyd et al., 2014; Portnyagin et al., 2019). These challenges can be circumvented by selecting large and

rapidly quenched inclusions (Ni et al., 2019; Su and Zhang, 2024). In this regard, inclusions hosted by olivine are considered to be more representative of the pre-eruptive, primitive melt (Hauri et al., 2011; He et al., 2025). However, melt inclusions only freeze in the volatile record at the time of inclusion formation, so any pre-entrapment magmatic processes (from mantle melting to fractional crystallization) must be accounted for to reconstruct primary melt and source compositions.

A widespread approach in geochemistry to avoid complicated reconstruction of the magmatic process is to use conservative elemental ratios, that is, elements that are incompatible in almost all crystallizing phases and, therefore, their relative abundances in the melt do not change with crystallization or during partial melting of the mantle. For reconstructing H contents, the H_2O/Ce ratio has been demonstrated to be a conservative index in terrestrial magmas, as H and Ce are both highly incompatible. Accordingly, their ratios remain constant during magmatic differentiation (Dixon et al., 2002; Michael, 1995; Saal et al., 2002). It follows that if the initial Ce concentration of the lunar mantle source is known, the H content of the mantle can be determined from the measured H_2O/Ce ratio of the melt inclusion. Using this approach, recent studies have concluded that the lunar mantle could be more "wet" than previously thought, as inferred water concentrations approach those of the Earth's upper mantle (e.g., Chen et al., 2015; Hauri et al., 2015; Su and Zhang, 2024). An example is Apollo 17 sample #74220 olivine-hosted inclusions, which retained high water concentrations (up to 1563 μg/g; Fig. 1; Su and Zhang, 2024) due to its rapid post-eruptive cooling (Ni et al., 2017). These results have led to a recent reinterpretation of the Moon's origin and evolution. Specifically, volatiles, especially water, somehow survived the high-energy impacts associated with Moon formation (Saal et al., 2008) or were supplemented by a late veneer (Albarède et al., 2013; Engels et al., 2024).

While melt inclusions likely preserve H contents better than any other lunar material, the effects of magmatic differentiation before entrapment of the melt inclusions need to be considered carefully. Magmas undergo a bewildering array of processes from the source region to the eruption. These include crystallization, mixing, assimilation, and recharge (DePaolo, 1981; Rooney et al., 2018). Although the importance of crystallization is obvious, magmatic recharge is also a first-order process in the formation and evolution of magma chambers (Albarède, 1985; O'Hara, 1977; O'Neill and Jenner, 2012; Steiner et al., 2024). Fractional crystallization alone may not be able to fractionate the relative abundances of highly incompatible elements, but recharge can give rise to anomalous compositions that complicate any reconstruction of primary compositions. For instance, recharge has often been used to explain the anomalous enrichment of highly incompatible elements relative to the compatible elements (Krans et al., 2024; O'Neill and Jenner, 2012), as well as the variation of highly incompatible element ratios (Lee et al., 2014; O'Hara, 1977) observed in various tectonic settings on Earth [e.g., mid-ocean ridge (Coogan and O'Hara, 2015; Rannou et al., 2006), arc magmas (Chiaradia et al., 2011; Lee et al., 2006), and intraplate setting (Yu et al., 2015; Yu et al., 2017)].

The cyclic variation of magma composition, as suggested by the complex zoning in phenocrysts, especially the reversed zoning of olivine and plagioclase (Donaldson and Brown, 1977; Luo et al., 2023; Wong et al., 2025), can be taken as evidence of replenishment of new, more primitive melt during the mineral crystallization. Although the number of samples from the Moon is relatively limited, previous studies have reported compositional zoning of lunar minerals for decades (e.g., Hargraves et al., 1970; Hollister et al., 1971). Previous studies reported oscillatory (e.g., Boyd and Smith, 1971; Burger et al., 2009; Crawford, 1973; Elardo and Shearer, 2014; Götze et al., 1999; Luo et al., 2023; Xue et al., 2019) and hour-glass sector zoning (Srivastava et al., 2024) of olivine, pyroxene and plagioclase in lunar returned mare basalt and basaltic meteorites, an observation that has been interpreted as resulting from magmatic recharge in various terrestrial settings (e.g., Ginibre et al., 2007; Streck, 2008; Xing and Wang, 2020). Although the crystallization kinetics involving cation diffusion and mineral growth can also explain the phenomenon (Lofgren et al., 2006; Milman-Barris et al., 2008), some authors believe the complex zoning, especially the repeated reversed zoning sections, reflect the cyclic change of melt composition (e.g., Elardo and Shearer, 2014; Luo et al., 2023; Xue et al., 2019), indicating that the magmatic recharge process operated in the lunar magma reservoirs from ~3.9 Gyrs (Srivastava et al., 2024; Xue et al., 2019) to ~2.0 Gyrs (Luo et al., 2023).

For the water-enriched lunar samples, such as Apollo 74220, no reports of reverse or oscillatory zoning in minerals have been documented yet. However, the short-scale complex zoning was observed in olivine from the Apollo orange glass sample 74001/2 (First et al., 2023; First et al., 2025), which could be related to the periodic change in melt composition because of the repeated replenishing and magma differentiation in the reservoir before eruption (e.g., Streck, 2008; Ubide et al., 2019). Given the proximity of sampling locations for 74001/2 core and 74220, and the similarities observed in their petrological texture of olivine (McIntosh et al., 2024), grain size distribution (e.g., Heiken and McKay, 1974), glass beads major element chemistry (e.g., Shearer et al., 2024), and age data (e.g., Husain and Schaeffer, 1973; Saito and Alexander, 1979), these samples may have originated from one pyroclastic event from the source (Gibson and Andrawes, 1978), and therefore the periodic magma refill may have also played a role in the evolution of Apollo 74220 reservoir.

More importantly, geochemical characteristics can further provide evidence for the existence of magmatic recharge. Numerous terrestrial studies demonstrate that certain indirect geochemical characteristics can also indicate the crucial role of magmatic recharge. Because of being effectively isolated from the rest of the melt reservoir, the inclusions generally exhibit more primitive composition (e.g., lower incompatible element concentrations) compared to the coexisting matrix and volcanic glass, as the latter should be the product of fractional crystallization if the magmatic system remains closed (e.g., Ding et al., 2025). For several cases, magmatic recharge has been proposed because the melt inclusions show similar or even more evolved compositions compared to the whole rock or residual glass (e.g., Anderson, 1976; Ding et al., 2025; Rhodes et al., 1979). We observed that Apollo 74220 olivine-hosted inclusions display similar concentrations of incompatible elements compared to the embayment and volcanic glass form the same sample (e.g., Ce concentrations of ~18–28 μg/g in glass and ~11–27 μg/g in the glassy inclusions after post-entrapment correction; same for the other rare earth elements and K; Chen et al., 2015; Ni et al., 2019; Fig. 1; Table S2). This indicates that the Apollo 74220 magma reservoir did not remain closed and therefore, recharging melt could counteract the evolutionary trend expected from fractional crystallization alone. In addition, the anomalous compositional trend, such as the relatively constant major element concentrations with the obvious variation of incompatible elements (e.g., O'Hara, 1977; O'Neill and Jenner, 2012; Steiner et al., 2022; Walker et al., 1979), was also observed in 74220 melt inclusions (e.g., Fig. 1C-D; Table S2). This trend is difficult to explain solely by olivine and ilmenite fractional crystallization proposed by the previous petrogenesis study of 74220 magma (McIntosh et al., 2024). However, the geochemical data align well with the evolution trend of recharge proposed by previous studies (e.g., Albarède, 1985; Lee et al., 2014; O'Hara, 1977).

Motivated by these lines of evidence suggesting the potential importance of magmatic recharge processes on the lunar magma reservoirs, here we evaluate the influence of recharge, a fundamental process in magma evolution, on the interpretation of lunar melt inclusion geochemistry. We primarily focus on Apollo 17 sample #74220 (Fig. S1; Table S2), which is commonly used to infer a relatively wet lunar mantle. We also extended our modeling to water and other available volatile element data from melt inclusions in Apollo 79135 and 15597 samples (Fig. 1A–B; Su and Zhang, 2024) in an effort to explain their volatile content. Melt inclusions in these samples, although not as water-rich as those in Apollo 74220, also showed elevated volatile/non-volatile trace element ratios. Our geochemical modeling shows that magmatic recharge, combined with fractional crystallization, can

significantly alter the lunar primary melt H_2O and H_2O/Ce estimates, as well as many other volatile and non-volatile incompatible elements, depending on the frequency of the recharge events. We argue that the lunar mantle water and other volatile element budget can be moderately to severely depleted compared to many recent estimates.

2. Methods

2.1. The general effects of magmatic recharge

The mass and composition of a magma reservoir are controlled by several processes, including crystal segregation, recharge, eruption/evacuation, and wall rock assimilation (e.g., Rooney et al., 2018). Here, we explore the effects of simultaneous magmatic recharge and fractional crystallization with varying proportions of eruption on lunar melt composition by the analytical equations in Lee et al. (2014) (Equations are provided in Supplementary materials). Continuous recharge in a simultaneously crystallizing magma reservoir results in progressive enrichment of incompatible elements in the melt because these elements are not partitioned into crystallizing phases, and in the buffering of compatible and major element concentrations in the melt because their abundances are replenished by the recharging melt (DePaolo, 1981). Compatible elements reach compositional steady state (a state where recharging melt balances the compositional variations caused by crystallization and eruption, such that the bulk composition of the magma reservoir does not change significantly with time or further recharge pulse) faster (i.e., with lower integrated recharge) than incompatible elements. Consequently, recharge generates incompatible element-enriched melts without significant depletion in compatible elements like Mg, giving the impression of a primitive melt derived from an enriched source (e.g., Apollo 74220 sample; Table S2). In particular, for incompatible elements, small differences in partitioning behavior become magnified with progressive recharge events, leading to fractionation of incompatible element pairs, complicating the use of their ratios as perfectly conservative tracers (Lee et al., 2014).

2.2. Model set-up

For recharge models, we assumed constant partition coefficients for each recharge event (e.g., Coogan and O'Hara, 2015; Lee et al., 2014; O'Neill and Jenner, 2012). This is not an unreasonable assumption given that the primary control on partition coefficients is temperature, and recharge tends to buffer the temperature and major element composition of a crystallizing magmatic system. The determination of elemental partition coefficients for parental melts of different volatile-enriched melt inclusions during their evolution within magma reservoirs will be detailed in subsequent sections. As the first-order approximation, we assume the composition of the recharging melt is equal to that of the initial melt in the reservoir (henceforth referred to as parental melt), given that both may originate from the same mantle source. As recharge in the reservoir continues with crystallization, the melt in the reservoir approaches a steady state composition (Eq. S7). Because time cannot be directly tracked, we track the progression of time through the number of "turnovers", which is the ratio of the total time-integrated mass of recharged melt to the original mass of the melt reservoir. Here, we calculate the evolution of Ce and H_2O in three scenarios: 1) pure fractional crystallization (FC), 2) simultaneous recharge and fractional crystallization (RFC), and 3) simultaneous recharge, eruption, and fractional crystallization (REFC). We compare our modeling results with the geochemical data of volatile-enriched, lunar melt inclusions.

3. Modeling the parental melt water content and mantle source for the 74220 melt inclusions

3.1. The compilation of 74220 melt inclusions

In Table S2, we compiled all available data of major elements, major volatile elements (H_2O, S, F, Cl), and their incompatible element counterparts (Ce, Dy, Zr, Ba) that are usually applied together as conservative element ratios, of the volatile-rich lunar melt inclusions (Chen et al., 2015; Hauri et al., 2011; Hauri et al., 2015; Ni et al., 2017; Su and Zhang, 2024).

The primary investigated samples are the most water-enriched lunar melt inclusions in the Apollo 74220 sample (Chen et al., 2015; Hauri et al., 2015; Ni et al., 2017; Su and Zhang, 2024). Some melt inclusions in 74220 are crystalline and were homogenized in the laboratory in previous studies, resulting in the loss of H_2O during this process, which necessitates further calibrations (Ni et al., 2019). In order to avoid the uncertainties involved in this correction, we only considered the naturally glassy inclusions (Fig. S1C-D). All melt inclusion data we compiled are olivine-hosted, and all host olivines show Mg# of 74–82, suggesting that they were not formed after eruption (Stephant et al., 2020). This is because the crystallization after eruption will make the concentration of incompatible elements in the melt show a negative correlation with host olivine Mg#, which was not observed here (Table S2). All inclusions experienced different degrees of post-entrapment crystallization (PEC), which severely altered their major element concentrations, such as MgO (transparent symbols; Fig. 1). We described our PEC correction methods in the Supplementary materials. We also provided the element concentrations after PEC correction (Fig. 1; Table S2). In addition to the major elements, we also recalculate the volatiles and other highly incompatible elements of the inclusions, assuming these elements do not enter olivine during PEC because of their extremely low partition coefficients between olivine and lunar basaltic melt (Chen et al., 2022; Potts et al., 2021; Table S3).

3.2. Choice of partition coefficients

The crystallizing mineral mode is required to calculate the bulk partition coefficients during recharge and fractional crystallization in the magma reservoir. We started from the well-studied Apollo 74220 sample. Previous studies observed that the compositional trend of 74220 melt inclusions overlaps with the trend of 74220 matrix glass and volcanic orange glass beads, and that melt inclusions are similar to or relatively more primitive compositions compared to the glass (Fig. 1C-D; Hauri et al., 2011). Here, we found similar major element concentrations between the 74220 orange glass and the inclusion after the post-entrapment correction. Compared to melt inclusion, the compositions of 74220 glass beads exhibit comparable to higher incompatible refractory element concentrations with varying degrees of loss of volatiles (Fig. 1). The orange glasses experienced further equilibrium and/or kinetic degassing during subsequent evolution and eruption (black arrow in Fig. 1 A-B). Given that the major element contents remained constant at steady state for most of the time in the modelling recharge process, we use high temperature phase equilibrium experiments based on the major element concentration of 74220 orange glass to constrain the average crystallizing mineral assemblage that may be in equilibrium with 74220 melt inclusions (Green et al., 1975; Krawczynski and Grove, 2012).

The experimental work by Krawczynski and Grove (2012) suggests the 74220 orange glass is saturated with olivine and orthopyroxene at ~1560 °C and 3.1 GPa for fO_2 below the IW buffer, which is close to the lunar redox state (Dygert et al., 2025; Ji and Dygert, 2023; Rutherford

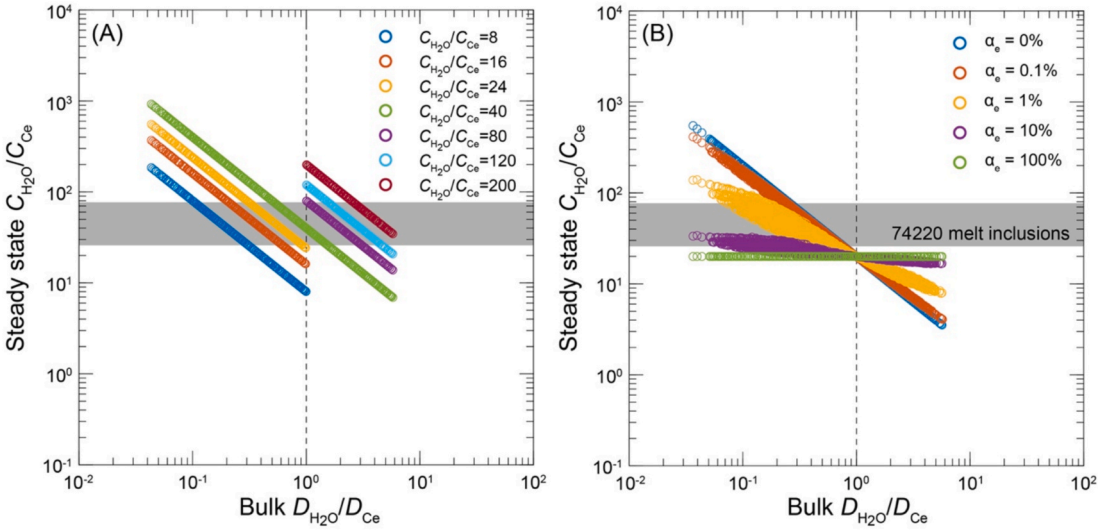

Fig. 2. The steady-state concentration ratio of H_2O and Ce (Eq. S7) as a function of bulk partition coefficient ratio of H_2O and Ce under the condition of recharge in the magma reservoir without (A) and with (B) melt eruption. The range of bulk partition coefficients for Ce (D_{Ce}) and H_2O (D_{H_2O}) is from the Monte Carlo simulations described in the Supplementary materials. The grey area represents the H_2O/Ce concentration ratio (C_{H_2O}/C_{Ce}) of Apollo 74220 melt inclusions (Table S2). Different colors in panel (A) represent different C_{H_2O}/C_{Ce} of the parental melt. Different colors in panel (B) represent different mass ratio (α; expressed as percentage) variations of melt removal to the parental melt during the REFC processes. The panel (B) shows that irrespective of the value of D_{H_2O}/D_{Ce}, the increased mass ratio of melt removal decreases the degree of fractionation between H_2O and Ce, thereby weakening the effect of recharge.

et al., 2017). Clinopyroxene and garnet are also observed as stable phases close to the liquidus at pressures higher than 3.1 GPa, and olivine always exists as a liquidus phase. An earlier study by Green et al. (1975) suggested that the 74220 melt is saturated with olivine, orthopyroxene, and clinopyroxene at 1520 °C and 3 GPa, but olivine is not a liquidus phase at > 3 GPa. Because previous experimental studies did not yield convergent results, we applied the pMELTS program at five different pressures (2.2, 2.4, 2.6, 2.8, 3.0 GPa) and simulated isobaric crystallization of 74220 orange glass composition starting from 1600 °C under the fO_2 of IW–1 (Table S4, Fig. S2). We realized that a previous study indicated that the existing thermodynamic models exhibit varying degrees of discrepancy when applied to compositions of lunar basalts and the corresponding oxygen fugacities compared to results of high pressure–temperature experiments (e.g., Astudillo Manosalva and Elardo,

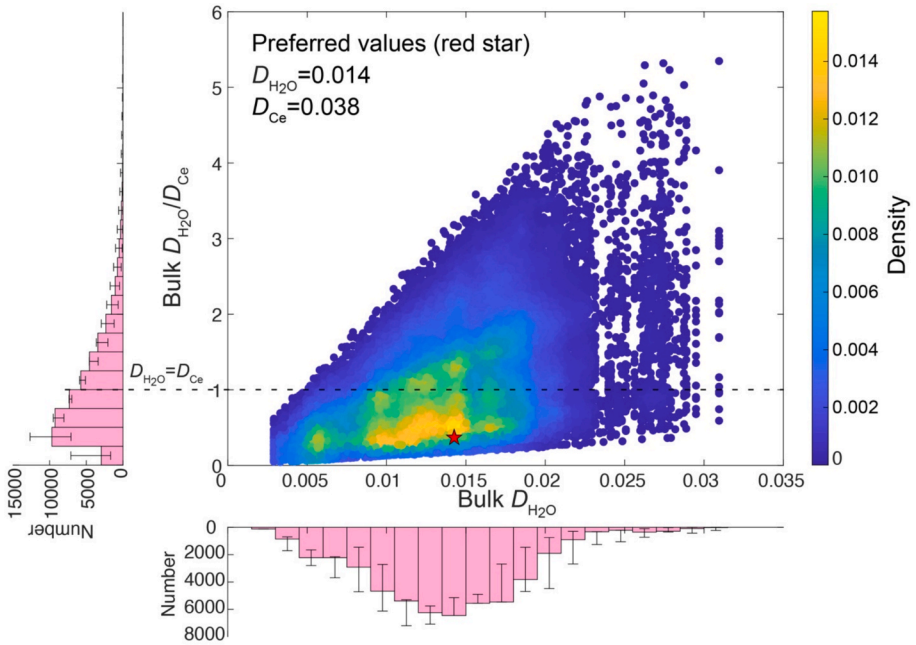

Fig. 3. The Monte Carlo simulations showing the bulk partition coefficient ratio of H_2O and Ce versus the bulk partition coefficient of H_2O. The bulk partition coefficients are estimated using a Monte Carlo method, where partition coefficients of Ce and H_2O between minerals and melt were randomly chosen from our compiled literature data (Table S3) and assuming the average crystallizing mineral assemblage is 15% olivine + 15% clinopyroxene + 70% orthopyroxene. The colors of the symbols present the density of the plotted data, and the yellow area is the place that represents the highest density. Two histograms show the data distribution of the Monte Carlo simulation results of 50,000 simulations; 29,229 out of 50,000 runs show D_{H_2O}/D_{Ce} values less than 1 (data lower than the dashed line). The red star represents the partitioning data applied in the main text, i.e., D_{H_2O}=0.014 and D_{H_2O}/D_{Ce}, =0.37, which corresponds to the peak in the histograms. The error bars of the histograms are the data distribution variations after considering the reported 2 sigma uncertainties of the compiled partitioning data (Table S3).

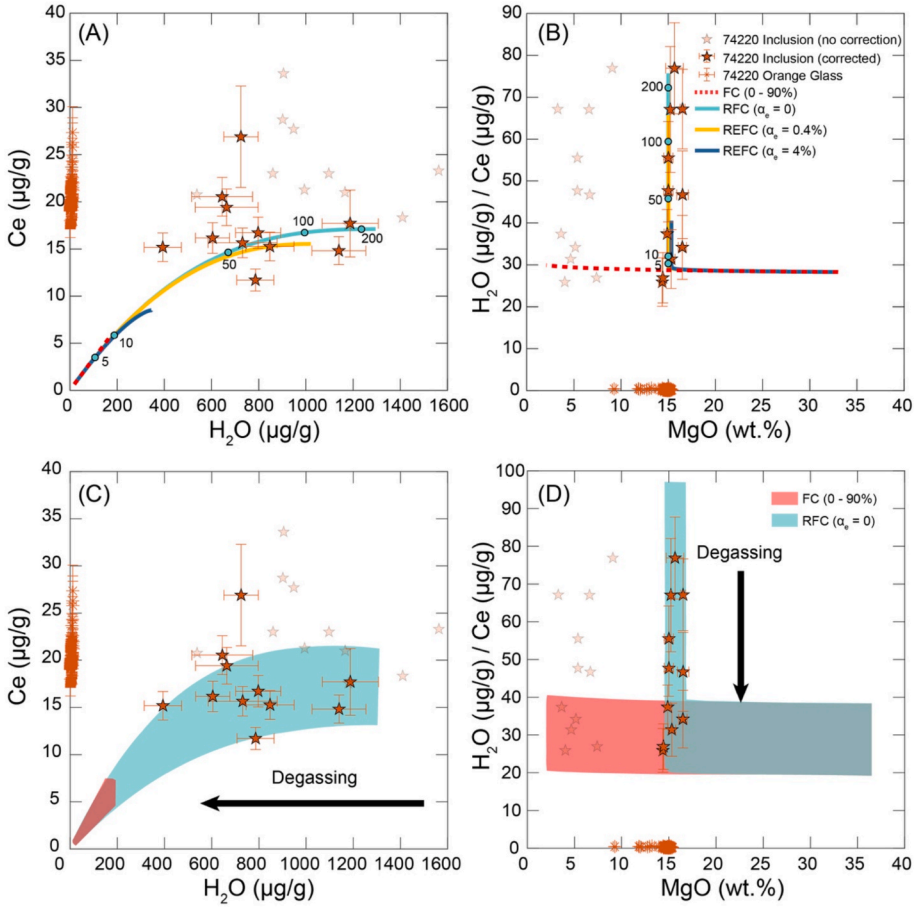

Fig. 4. Concentrations of Ce versus H_2O (A and C) and H_2O/Ce versus MgO (B and D) for melt inclusions in Apollo 17 sample 74220, along with the orange glasses in 74220 for comparison. Also shown in (A) and (B) are model trends for fractional crystallization (FC; red dashed line), recharge and fractional crystallization (RFC, cyan solid line), and recharge and fractional crystallization with 0.4% and 4% mass of evacuation trend (REFC, yellow and blue solid lines). (C) and (D) present calculation where the parental melt compositions are varied in the RFC model to reproduce the two most water-enriched inclusions [74220 A2 (Hauri et al., 2011) and 74220-OL7 (Su and Zhang, 2024); Table S2] after 200 turnovers (cyan areas), taking into account the 2σ uncertainties. The cyan circles and the numbers next to them in (A) and (B) represent the number of turnovers in the RFC model. The semitransparent stars represent the compositions of inclusions before the PEC correction. The arrows in panels (C) and (D) suggest the degassing trend that may exist during the magma evolution and post-eruption, which is closely related to the water depletion observed in the orange glass (Saal et al., 2008). The resultant H_2O and Ce concentrations range in the parental melt of 74220 inclusions are 15–19 μg/g and 0.5–0.8 μg/g, respectively. The required MgO content ranges from 32.4 to 36.5 wt%. The FC model trends are shown as red dotted lines (A and B) or red shaded areas (C and D) for comparison.

2024). However, previous application of the MELTS family of algorithms to lunar samples has been shown to provide useful constraints on mantle source lithology, mantle melting conditions, and lunar magma crystallization (e.g., Fagan et al., 2014; Srivastava et al., 2022; Srivastava et al., 2024). We tracked the crystallization of olivine, orthopyroxene, clinopyroxene, and garnet by pMELTS, and the results suggested the 74220 orange glass is saturated with garnet and orthopyroxene at ~1560 °C and 2.9 GPa, and clinopyroxene joins the crystallization assemblage at lower pressures. However, from 2.2 to 3.0 GPa, olivine does not occur as the liquidus phase, suggesting that the role of olivine during the evolution of 74220 orange glass may be limited. Due to the inconsistencies between previous experimental studies and the different results indicated by pMELTS modeling, the average crystallizing mineral mode cannot be well constrained. Therefore, in our main calculations, we assume the dominant phase in the crystallizing mineral assemblage is orthopyroxene (15% olivine + 15% clinopyroxene + 70% orthopyroxene), and then tested the scenario with 5% garnet in the mineral assemblage.

With the assumed crystallizing mineral assemblage, we performed Monte-Carlo simulations using a wide range of the mineral-melt partitioning data from fifty experimental studies and one lunar mineral-melt inclusion study (Table S3) to calculate the bulk partition coefficients. We investigated the effect of variations in bulk partition coefficients on H_2O and Ce concentrations in the melt based on all possible bulk partition coefficients suggested by Monte-Carlo simulations after 50,000 samplings (Fig. 2). If D_{H_2O}/D_{Ce} is exactly equal to 1, the H_2O and Ce will not fractionate from each other during recharge, and the steady state C_{H_2O}/C_{Ce} is equal to the initial value (dashed line in Fig. 2A). If the bulk partition coefficient ratio is less than 1, the recharge will increase C_{H_2O}, C_{Ce}, and C_{H_2O}/C_{Ce} gradually. In this case, the high C_{H_2O}/C_{Ce} melt can be reproduced by the parental melt with low C_{H_2O}/C_{Ce} (Fig. 2A). If D_{H_2O}/D_{Ce} is greater than 1, however, the recharge will decrease C_{H_2O}/C_{Ce} gradually, hence the melt can evolve from high C_{H_2O}/C_{Ce} to low C_{H_2O}/C_{Ce} in the reservoir even without degassing (Fig. 2A). In order to find the most probable combination in bulk partition coefficients distribution, we plotted simulations of each element in density plots (Fig. 3 and S3-S4). The Monte Carlo results suggest the most likely bulk D_{H_2O} is between 0.014 and 0.015, D_{H_2O}/D_{Ce} is between 0.25 and 0.5, and ~60% of simulations yield D_{H_2O}/D_{Ce} less than 1, i.e., H_2O is more incompatible than Ce. Based on the density plot of the Monte Carlo simulation (Fig. 3), we chooseD_{H_2O} = 0.014 andD_{Ce} = 0.038 (D_{H_2O}/D_{Ce} = 0.37) in the following models.

Table 1
Compositions of volatile and refractory elements in the parental melt of 74220 inclusions calculated by the RFC and REFC models, as well as volatile abundances in the source region.

No-garnet[a], RFC	Parental melt (μg/g)							
	H_2O	Ce	S	Dy	F	Zr	Cl	Ba
	15–19	0.5–0.8	3–6	0.5–0.8	1.1–2.0	5–8	0.01–0.03	0.50–0.73
	Source region (5–30% batch melting)[b]							
	D_{H_2O}	H_2O (μg/g)	D_S	S (μg/g)	D_F	F (μg/g)	D_{Cl}	Cl (μg/g)
	0.005–0.01	1–6	0.1–0.2	0.4–3	0.03–0.06	0.1–0.7	0.00005–0.00015	0.001–0.009
5% garnet[a], RFC	Parental melt (μg/g)							
	H_2O	Ce	S	Dy	F	Zr	Cl	Ba
	13–16	0.2–0.7	3–6	1.9–2.8	1.0–1.7	7–11	0.01–0.03	0.50–0.73
	Source region (5–30% batch melting)[b]							
	D_{H_2O}	H_2O (μg/g)	D_S	S (μg/g)	D_F	F (μg/g)	D_{Cl}	Cl (μg/g)
	0.005–0.01	1–5	0.1–0.2	0.4–3	0.03–0.06	0.1–0.6	0.00005–0.00015	0.001–0.009
No-garnet[a], REFC[c]	Parental melt (μg/g)							
	H_2O	Ce	S	Dy	F	Zr	Cl	Ba
	59–73	1.0–1.6	18–37	0.8–1.2	2.7–4.7	10–16	0.05–0.23	3.03–4.44
	Source region (5–30% batch melting)[b]							
	D_{H_2O}	H_2O (μg/g)	D_S	S (μg/g)	D_F	F (μg/g)	D_{Cl}	Cl (μg/g)
	0.005–0.01	3–22	0.1–0.2	3–16	0.03–0.06	0.2–1.6	0.00005–0.00015	0.003–0.07

[a] Two different crystallizing assemblages, one containing no garnet and the other containing 5% garnet. For RFC, we modeled the magma reservoir with 200 turnovers for all volatiles.
[b] The partition coefficients of volatiles are from Hauri et al. (2011). More calculation details are given in the Supplementary Materials.
[c] 4% mass of evacuation in the REFC model; because the REFC model requires fewer turnovers (~60) to reach the steady state of H_2O, we applied 60 turnovers for all volatiles (Fig. S6).

3.3. The effects of magmatic recharge

The modeling results, presented in Fig. 4, show that under FC only, the MgO concentration of the melt progressively decreases, and Ce and H_2O increase. However, Ce and H_2O do not fractionate from each other efficiently, even after 90% of the melt solidifies (red dashed line in Fig. 4A–B). By contrast, under RFC (cyan lines in Fig. 4A–B), the concentrations of compatible elements like MgO decrease first and approach a steady state due to buffering by recharging melt. Similarly, Ce and H_2O initially increase, but eventually reach a steady state as well. Two important observations are – (1) because incompatible elements reach the steady state later than compatible elements (i.e., the partition coefficient of element is negatively correlated with the number of turnovers required to reach the steady state; Eq. S6), melts with high Ce and H_2O for a given MgO can be achieved giving the false impression of primitive melts with anomalously high Ce and H_2O. (2) Because H_2O is taken to be more incompatible than Ce, based on the argument presented above ($D_{H_2O}/D_{Ce} < 1$; Fig. 3), Ce and H_2O can fractionate with respect to each other significantly, resulting in H_2O/Ce ratios independent of the source composition (cyan line in Fig. 4B). In Fig. 4, we show that RFC can reproduce almost all 74220 melt inclusions, among which inclusions with the highest H_2O/Ce ratios may have been captured into the host minerals after more turnovers, or experienced less post-eruption water loss (Zhang, 2020).

The high H_2O/Ce ratios generated by RFC require numerous turnovers. A steady state, for example, is achieved after 200 turnovers (cyan circles in Fig. 4A–B). In general, this number of turnovers is not unreasonable. A significant number of recharge cycles have also been suggested in tracking the evolution of K in mid-ocean ridge magma reservoirs on Earth (Coogan and O'Hara, 2015). A high turnover number typically indicates a deep and long-lived reservoir (Lee and Liu, 2021) or a high magmatic flux through small magma bodies. There is no good way to estimate typical magma reservoir sizes that gave rise to Apollo 74220 samples, but given that some magma bodies on Earth that were originally thought to be kilometer-scale may be small and may exist in the form of sills (Lee et al., 2022), it could be expected if 74220 inclusions evolved in a small reservoir. Further discussion of the effects of turnover numbers is provided in Section 3.5.

To evaluate the sensitivity of our models to the parental melt's H_2O, Ce, and MgO content, we varied the parental melt's composition and applied the RFC model to reproduce the compositions of the two most water-enriched 74220 inclusions (1188 ± 119 and 1139 ± 114 μg/g H_2O after PEC correction; Table S2), considering propagated uncertainties. We assumed the melt in the reservoir has approached a compositional steady state (~200 turnovers) and considered the range of plausible initial H_2O and Ce concentrations to be 15–19 μg/g and 0.5–0.8 μg/g, respectively. The H_2O/Ce ratio of the parental melt calculated here is as low as ~19–38, one-quarter to half of the values estimated from 74220 melt inclusions when H_2O/Ce was assumed not to fractionate (Chen et al., 2015; Hauri et al., 2015; Ni et al., 2019). The MgO contents of the parental melt are calculated to be 32.4. to 36.5 wt% with the above assumed crystallizing mineral assemblage, and can be 25.8 wt% or even lower [similar to the melts that are in equilibrium with primitive lunar mantle cumulate prior to the solidification of 52% of the magma ocean in Rapp and Draper (2018)], depending on the weight percentage of olivine in the assemblage (Fig. S2B). Irrespective of the absolute value, the high MgO in the parental melt must be generated from highly primitive mantle cumulates (for more discussion see Supplementary Materials). Within the above major and trace element ranges, almost all inclusions are reproduced by the parental melt (Fig. 4C–D).

To reconstruct the water concentration in the source region, we can either apply a conservative volatile/refractory ratio (Hauri et al., 2015; Ni et al., 2019) or a reconstruction of magmatic processes (Hauri et al., 2011; Stephant et al., 2020). The first approach requires that the contents of refractory elements in the source region are known. However, tracking elemental contents in the lunar mantle is challenging because of the complex secondary processes that may lead to mantle heterogeneity during and after lunar magma ocean solidification (e.g., mantle overturn; Hess and Parmentier, 1995). Even for the application to the lunar primitive mantle, previous studies proposed bulk silicate Moon with refractory trace element concentrations ranging from 4-5 × CI chondrite (Snyder et al., 1992; Taylor et al., 2006), to ~2.5 × CI (bulk silicate Earth-like; Fu and Jacobsen, 2024; Taylor, 1982), to even 1 × CI chondrite (Ji and Dygert, 2023; Rapp and Draper, 2018), which would introduce significant computational uncertainties. To avoid the above

Table 2
Modeled volatile element concentrations in the parental melt and mantle source of Apollo 74220 and 79135 melt inclusions from this study compared to previous studies.

	Parental melt					Mantle source[a]				
	H_2O (μg/g)	S (μg/g)	F (μg/g)	Cl (μg/g)	Ref.	H_2O (μg/g)	S (μg/g)	F (μg/g)	Cl (μg/g)	Ref.
Apollo 74220 melt inclusions										
Measurement[b]	270–1202	447–884	36.6–72.1	0–2.38	Hauri et al. (2011)	79–409	193–352	7–26	0.14–0.83	Hauri et al. (2011)
RFC + 200 turnovers	15–19	3–6	1.1–2.0	0.01–0.03	This study	1–6	0.4–3	0.1–0.7	0.001–0.009	This study
REFC + 60 turnovers	59–73	18–37	2.7–4.7	0.05–0.23	This study	3–22	3–16	0.2–1.6	0.003–0.07	This study
RFC + 10 turnovers	100–128	36–71	4.2–7.3	0.11–0.48	This study	6–39	5–31	0.3–2.5	0.006–0.024	This study
REFC + 10 turnovers	123–157	44–87	5.1–8.9	0.14–0.59	This study	7–48	6–38	0.4–3.0	0.007–0.178	This study
Apollo 79135 melt inclusions										
Measurement[b]	450–694	259–650	43.3–70.5	1.36	Su and Zhang (2024)	37–153	91–205	2.2–10.6	0.05–0.29	This study
RFC + 200 turnovers	9–12	5–7	1.1–2.2	0.06–0.09	This study	1–4	1–3	0.1–0.8	0.0003–0.003	This study
REFC + 60 turnovers	35–43	27–37	2.6–5.4	0.05–0.07	This study	2–13	4–15	0.2–1.8	0.002–0.02	This study
RFC + 10 turnovers	62–76	53–72	4.0–8.3	0.11–0.15	This study	3–23	8–31	0.3–2.9	0.005–0.044	This study
REFC + 10 turnovers	76–93	65–88	4.8–10.1	0.13–0.18	This study	4–29	9–39	0.4–3.5	0.007–0.054	This study

[a] The calculations were conducted following the same methods described in Table 1, applying partition coefficients of volatiles and lunar mantle melting degree estimated by Hauri et al. (2011).
[b] Values after PEC corrections.

uncertainties, we apply the second method here. We assume that the parental melt is generated by 5–30% batch melting of the source region (Hauri et al., 2011). The calculation results suggest that the water abundance in the source region could be as low as ~1–6 μg/g (Table 1). Interestingly, these concentrations are similar to those estimated for the mantle of ~2.0 Ga Chang'e-5 basalts (Hu et al., 2021). However, a consideration of magma recharge has not been made for Chang'e-5's magma reservoir. Hence Chang'e-5 source may still be drier than the source of Apollo 74220. We also tested the scenario that a small amount of garnet appears in the crystallizing phase assemblage, as suggested by experimental studies (Green et al., 1975; Krawczynski and Grove, 2012). For H_2O and Ce, the effect (e.g., 5 wt% crystallizing garnet) is very limited (Fig. S5), and we can still reproduce the compositions of 74220 inclusions by RFC processes with a similar recharging partial melt composition (Table 1). This suggests that if recharge is important on the Moon and many turnover events took place during fractional crystallization, the parental melt of 74220 could be much more water-depleted than previously thought (as low as ~13 μg/g), which is contrary to the highly water-enriched melt suggested by previous studies (Hauri et al., 2011; Saal et al., 2008).

3.4. The effects of eruption on the water budget of parental melt affected by recharge-fractional crystallization

We note that the H_2O concentrations of both parental melt and the source region estimated above are likely lower bounds, as we did not account for the effects of eruption above. Including eruption or evacuation (REFC) does not alter the overall elemental trends from RFC, but

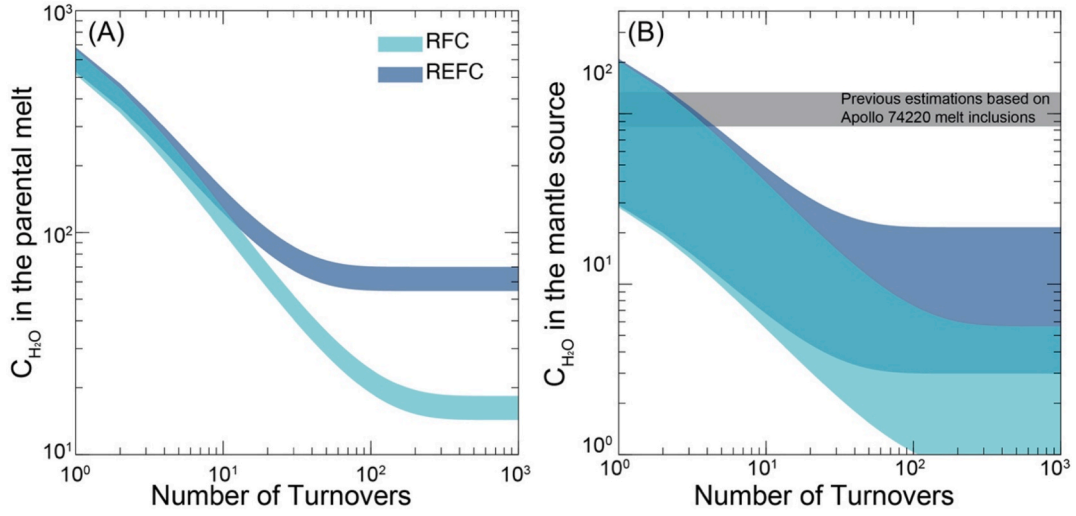

Fig. 5. Concentrations of H_2O (A) in the parental melt and (B) in the mantle source of 74220 melt inclusions versus the number of turnovers in the magma reservoir. The RFC and REFC models are the same as those in Fig. 4, while the number of turnovers in the reservoir is varied in order to calculate the required concentrations of H_2O in the parental melt that is able to reproduce the two most water-enriched 74220 melt inclusions (Table S2). The width of the bands in panel (A) capture the analytical uncertainties of H_2O in the melt inclusions, while the band widths in panel (B) capture the propagation of analytical uncertainties and lunar mantle melting degrees (5–30% batch melting; Hauri et al., 2011). The estimated H_2O concentrations of the primitive lunar mantle based on 74220 inclusions are provided for comparison and are taken from Table S1.

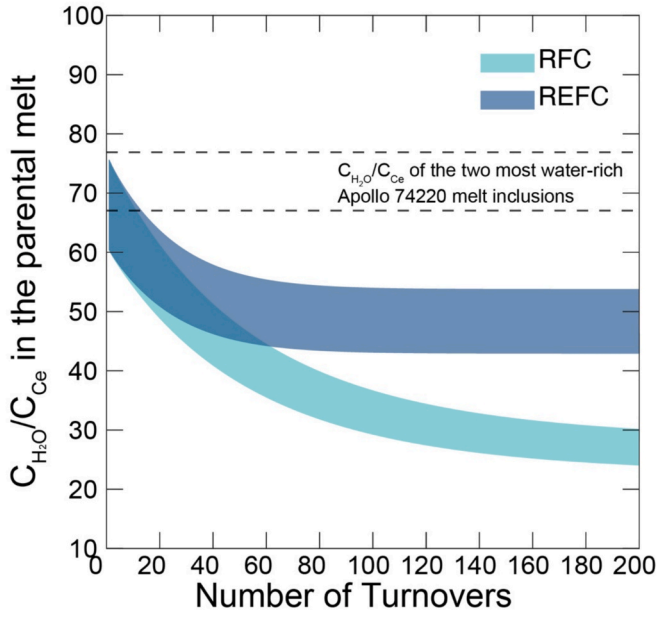

Fig. 6. H_2O/Ce in the parental melt versus the number of turnovers in the magma reservoir. The RFC and REFC models, along with the calculation of turnover numbers, are identical to those in Fig. 4. The widths of the bands correspond to the analytical uncertainties of H_2O and Ce in the melt inclusions, while dashed lines represent the H_2O/Ce ratios of the two most water-enriched 74220 melt inclusions (Table S2).

simultaneous eruption or evacuation weakens the total effect of recharge on enriching incompatible elements and fractionating their relative abundances (compare yellow and blue lines in Fig. 4A-4B; Fig. 2B). Coogan and O'Hara (2015) proposed a recharge model with 4% eruption mass ratio as a suitable assumption for interpreting the geochemical characteristics of mid-ocean ridge basalts. Due to differences in model set-up (e.g., calculation of recharge cycle), their eruption ratio may correspond to a higher eruption ratio defined here (Eq. S2). However, the mid-ocean ridge can create more efficient melt transport conduits than on the Moon due to its tectonics, and thus the mass ratio of eruptions in the lunar mantle could be much lower. Because of the lack of valid constraint on the eruption rate in the deep lunar mantle, we started with a REFC process with an eruption flux of 4% relative to total fluxes (crystallization and evacuation/eruption; Fig. 4A-4B), and exhibited the effect of variable eruption ratios in Fig. 2B. The 4% of eruption ratio will not significantly change the required MgO concentrations. However, H_2O and Ce both reach the compositional steady state after ~60 turnovers, which is earlier than without eruption (Eq. S6). Including eruption increases the required H_2O and Ce abundances in the parental melt to 55–70 μg/g and 1.0–1.6 μg/g, respectively (Fig. S7), corresponding to a source region of 3–22 μg/g H_2O (Table 1), still lower than the estimates from previous studies (Tables 2 and S1).

3.5. The effects of the frequency of recharge events

The number of turnovers in the magma reservoir is a key factor controlling the calculated H_2O concentrations in the parental melt, and consequently those in the mantle source. However, the number of possible turnovers in the lunar magmatic systems remains unconstrained. The turnovers in the magma reservoir depend on several variables, such as the degree of lunar mantle melting, as well as the size and structure of the reservoir. In the preceding sections, we allowed the turnover or recharge events to be as high as needed to reach steady state for H_2O and H_2O/Ce. Although the necessary turnover numbers of 60–200 (REFC and RFC, respectively) are not unreasonable, it is also plausible that 74220 melt inclusion entrapment took place after less number of turnover events and perhaps before the incompatible elements reached compositional steady state.

Therefore, to evaluate the effects of this parameter, here we examined how sensitive the H_2O concentrations and the H_2O/Ce ratio of the parental melt are to variations in the turnover number. In both the RFC and REFC models, reproducing the two most water-rich 74220 melt inclusions [74220 A2 (Hauri et al., 2011) and 74220-OL7 (Su and Zhang, 2024); Table S2] requires H_2O concentrations in the parental melt decrease with increasing turnover number (Fig. 5A). Notably, after only ~4–5 turnovers (Fig. 5B), the estimated H_2O concentrations in the lunar mantle falls below previous values derived from the 74220 inclusions (84–133 μg/g; Table S1). This suggests that, even if only a small number of magma reservoir turnovers took place, the estimated H_2O concentrations in the lunar mantle will drop significantly. For example, only with 10 turnovers, the estimated water content of the 74220 melt inclusion source becomes 6–39 μg/g and 7–48 μg/g for RFC and REFC model respectively (Table 2), which is distinctly lower than the previous estimates of 84–133 μg/g (Ni et al., 2019; Su and Zhang, 2024).

While the H_2O content of the parental melt starts to drop significantly only after a small number of recharge events (Fig. 5), affecting the H_2O/Ce ratio of the melt requires a relatively greater number of turnovers. However, even prior reaching a steady state, the recharge process acting in tandem with fractional crystallization can still elevate the H_2O/Ce of the resulting melt significantly above that of the parental melt. After ~13 turnovers, the parental melt exhibits H_2O/Ce ratios lower than those of most H_2O-rich melt inclusions, reflecting divergence between the melt and the source region in terms of the conservative elemental ratios (Fig. 6).

4. Other volatiles in the lunar mantle source of 74220 melt inclusions

Similar to H_2O and Ce, magmatic recharge must affect other incompatible element pairs commonly used to reconstruct source volatiles. These include volatile/refractory element pairs, such as S/Dy, F/Zr, and Cl/Ba (e.g., Hauri et al., 2015). For all these elemental ratios, we found that the volatile element was more incompatible than the paired refractory element using the Monte Carlo method described above (Fig. S3). Some of the above elements may be more incompatible than Ce and H_2O (e.g., Ba, Cl), requiring more turnovers to reach the steady state. To remain consistent with our above modeling, calculations were performed for 200 turnovers. Both volatile and refractory elements, as well as the elemental ratio increase with recharge, fitting the characteristics of 74220 melt inclusions (Fig. 7). Fractionation by recharge between S and Dy requires the absence of sulfide precipitation during the evolution of 74220, which has been confirmed by sulfide saturation experiments (Ding et al., 2018; Steenstra et al., 2018) and sulfur isotope study (Saal and Hauri, 2021). Still assuming the batch melting degree of the source is 5–30%, the required S, F, and Cl abundances in the source are 0.4–3 μg/g, 0.1–0.7 μg/g, and 0.001–0.009 μg/g in RFC model, whereas the abundances need to be increased to 3–16 μg/g, 0.2–1.6 μg/g, and 0.003–0.07 μg/g, respectively if the REFC processes with 4% mass of evacuation is taken into account (Table 1; Fig. S8), remaining below estimates from prior studies (Tables 2 and S1). The estimated S, F, and Cl abundances of the mantle source, assuming only 10 turnovers, are provided in Table 2.

5. Implications for other incompatible elements in the source of 74220 melt inclusions

Although our RFC and REFC models can explain the volatile element enrichment and volatile-to-non-volatile trace element ratios of 74220 melt inclusions, it is crucial to evaluate whether the recharge process is consistent with other geochemical attributes of the 74220 melt inclusions.

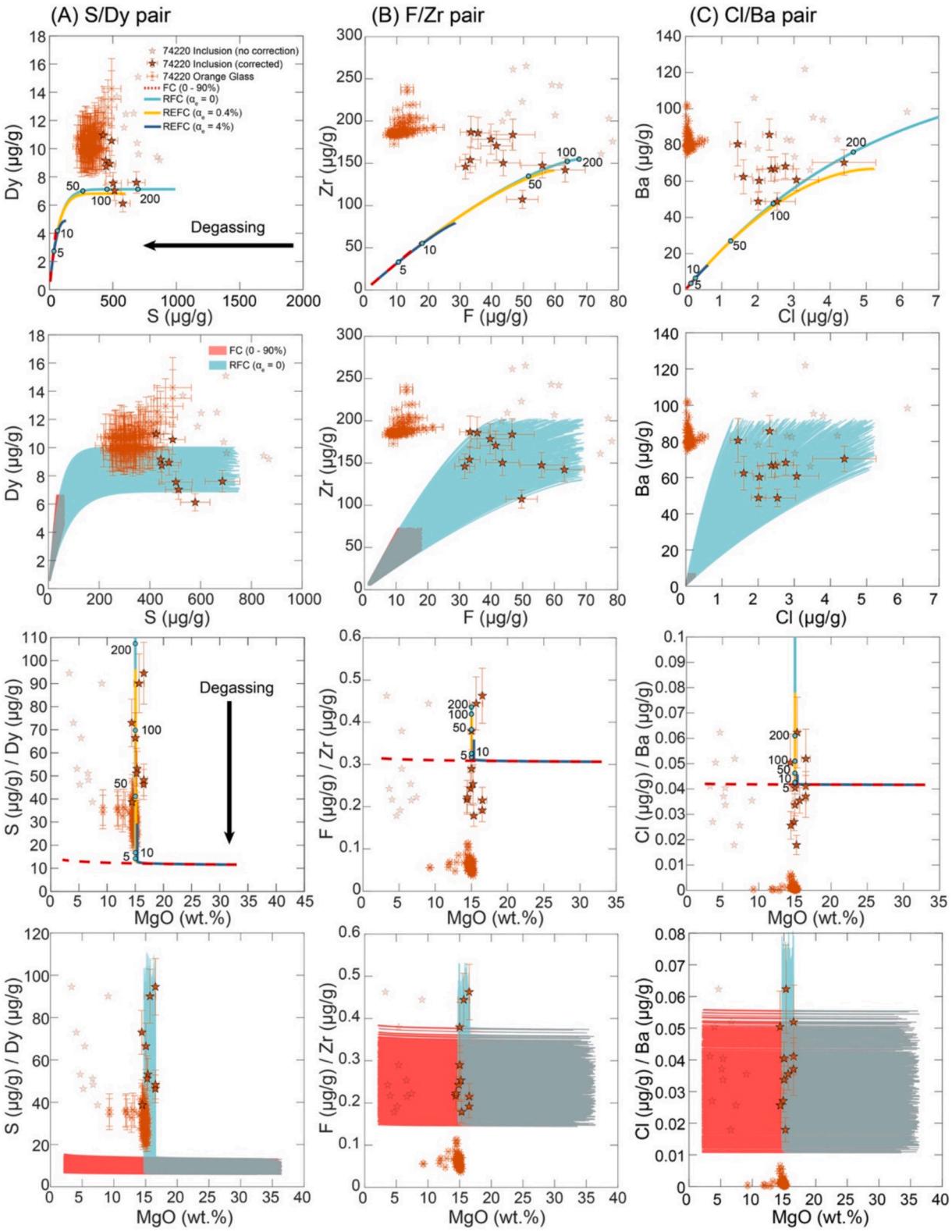

Fig. 7. Concentrations of (A) Dy versus S, and S/Dy versus MgO, (B) Zr versus F, and F/Zr versus MgO, and (C) Ba versus Cl, and Cl/Ba versus MgO for melt inclusions in Apollo 17 sample 74220, as well as the orange glasses in 74220 for the comparison. For F and S, we employ the Monte Carlo method to reproduce the compositions of the two most water-enriched inclusions [74220 A2 (Hauri et al., 2011) and 74220-OL7 (Su and Zhang, 2024)], the same samples as we utilized in Fig. 4C-4D. For Cl, the above two samples cannot present the most volatile enriched sample, so we add 74220-OldOl2 (Ni et al., 2017) for Cl as the modeling targets. All symbols and modeling methods are the same as in Fig. 4.

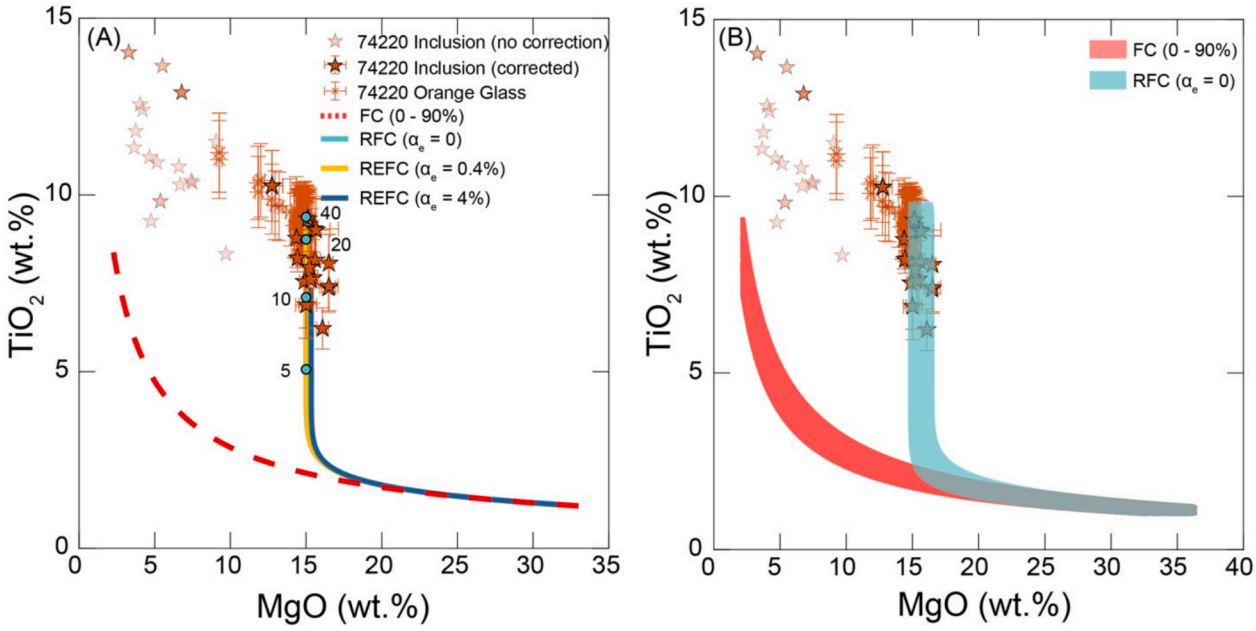

Fig. 8. Concentrations of MgO versus TiO_2 for melt inclusions and orange glasses in Apollo 17 sample 74220 compared with various magma differentiation models. (A) Relatively high TiO_2 concentrations in 74220 inclusions are successfully reproduced by RFC processes from a parental melt with low TiO_2 concentration. Only after ~20 turnovers, the TiO_2 contents can approach the compositional steady state. (B) Monte Carlo method reproducing the compositions of the two most water-enriched inclusions, similar to what is presented in Fig. 4C-4D. The required TiO_2 concentrations in the parental melt of 74220 inclusions are 1.0–1.3 wt%, if the crystallizing mineral assemblage contains no garnet. All symbols and modeling methods are the same as in Fig. 4.

5.1. *Ti enrichment in 74220 melt inclusions*

Another characteristic of the volcanic glass and melt inclusions collected in the 74220 pyroclastic deposit is the high-Ti signature (TiO_2 = 6.22–12 53 wt%; Hauri et al., 2015; Table S2). McIntosh et al. (2024) attributed the elevated Ti concentrations to an ilmenite-enriched cumulate mantle source and subsequent crystallization of olivine and ilmenite. However, in our recharge model, the crystallizing minerals should be buffered by the recharging melt, a process in an open system that is clearly different from magmatic differentiation in a closed system. Our recharge model suggests that the high TiO_2 concentrations of 74220 can result from a moderately low-TiO_2 parent melt (1.0–1.3 wt%; Fig. 8 and Table S2), without requiring a large amount of ilmenite in the source. Only after ~20 turnovers, our model produces a steady state for the TiO_2 contents.

5.2. *Implications for REEs*

The 74220 melt inclusions display a relatively flat and elevated Rare Earth Element (REE) pattern (Fig. S1; Chen et al., 2015; Hauri et al., 2015; McIntosh et al., 2024; Ni et al., 2017; Su and Zhang, 2024). Therefore, for the RFC or REFC process to be important for explaining volatile budgets, it also needs to explain the REE patterns. The REE contents of 74220 inclusions have been interpreted to involve mantle hybridization with an enriched late-stage magma ocean cumulate source (e.g., McIntosh et al., 2024). With the partition coefficient data recommended by Monte-Carlo simulation, parental melt requires a light REE depleted pattern (Fig. S9), in order to balance the heavy-REE preferred crystallized minerals and generate a relatively flat 74220 melt inclusions REE pattern (Fig. S1). A small amount of garnet in the crystallized assemblage will return an even more heavy-REE enriched parental melt (Fig. S9). However, both scenarios are consistent with our finding that the source of the volatile-enriched lunar melt inclusions might be primitive, and that recharge from a volatile-depleted cumulate mantle could have played a key role in the evolution of lunar melts.

6. Other volatile-enriched lunar melt inclusions

In our study, we focused primarily on the melt inclusions from the Apollo 74220 sample because these data yielded some of the highest estimations of water and volatile content for the Moon. However, a recent study by Su and Zhang (2024) reported that the melt inclusions in Apollo 15597 and 79135 also exhibit comparatively high H_2O/Ce ratios, closing the previously observed gap in H_2O/Ce between inclusions in 74220 and other Apollo samples. Here we show that, similar to that for74220 samples, the relatively elevated H_2O/Ce, as well as other volatile/refractory element ratios, of inclusions in 15597 and 79135 can also be explained not only by the characteristics of the source region, but by magmatic recharge (Fig. 9).

Su and Zhang (2024) investigated seven olivine-hosted melt inclusions in Apollo 79135, and found that the compositions of these inclusions and their olivine host exhibited a bimodal distribution (e.g., Fo_{80} and Fo_{71} olivine). Trace elements and volatile compositions were reported for three of them, whereas one of them (79135-OL11-2) lacked major elements and the Mg# data for the host olivine. We, therefore, applied the PEC correction to 79135 melt inclusions and utilized both PEC correction values of inclusions in olivine with Fo# of 80 and 71 to correct 79135-OL11-2. Based on the olivine Fo values employed, we assumed that the MgO composition of 79135-OL11-2 was identical to that of 79135-OL1 (host olivine Fo#=80) and 79135-OL7 (host olivine Fo#=71) inclusions, respectively. Volatile-rich inclusions from Apollo 15597 are pyroxene-hosted with highly fractionated compositions (e.g., MgO < 0.2 wt%; Su and Zhang, 2024). It is, therefore, difficult to estimate the primitive melt compositions of these extremely evolved melts by PEC correction and magma evolution reconstruction. However, the PEC correction will not significantly alter the commonly applied conservative volatile/refractory ratio, and thus, we can still uncover valuable clues about the volatile content of the lunar mantle from these inclusions.

Regarding the possible crystallizing mineral assemblage during the evolution of Apollo 79135 inclusions, although there is no genetic association between 79135 and 74220 (Su and Zhang, 2024), due to the

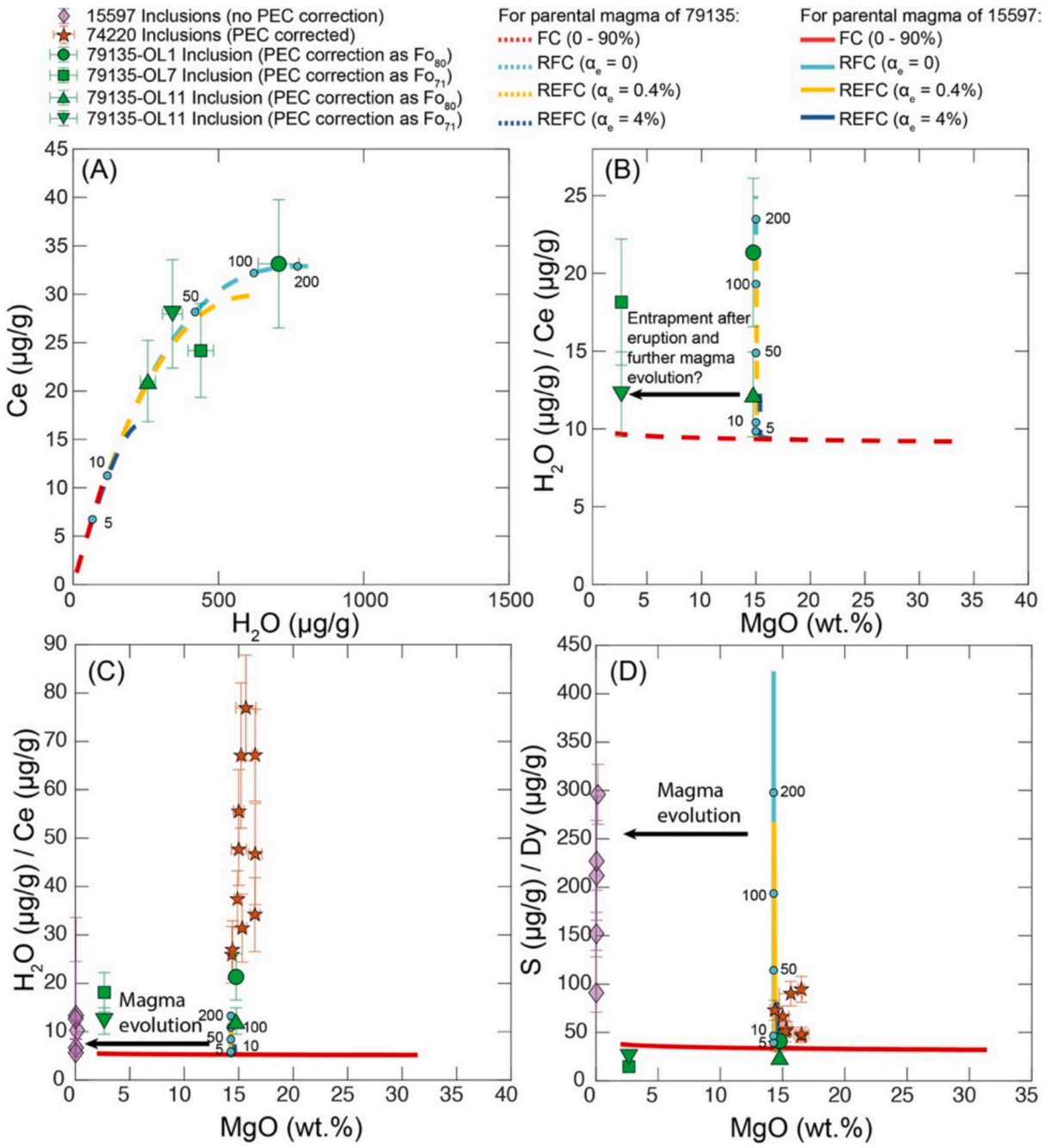

Fig. 9. (A-B) Concentrations of Ce versus H_2O and H_2O/Ce versus MgO for melt inclusions in Apollo 17 sample 79135. Also plotted are magma evolution models for fractional crystallization (FC; red lines), recharge and fractional crystallization (RFC, cyan lines), as well as recharge and fractional crystallization with 0.4% and 4% mass of evacuation trend (REFC, yellow and blue lines). (C-D) H_2O/Ce versus MgO and S/Dy versus MgO for melt inclusions in Apollo 15 sample 15597. All data of 79135 and 15597 inclusions are from Su and Zhang (2024) and are listed in Table S2.

lack of studies reporting the petrogenesis of 79135 volcanic glass as well as the presence of the 74220-type orange glass in 79135 (Simon et al., 1990), we assumed the crystallizing mineral assemblage of 79135 inclusions is the same as that of the 74220 inclusions. Because of the highly evolved compositions of the melt inclusions in Apollo 15597, reconstructing their original melt composition and crystallizing mineral assemblage is extremely challenging. Likewise, as the first-order estimation, we assume the recharging melt of 15597 originated from a mantle source similar to that of 74220 and 79135 in the subsequent modeling.

Application of our recharge model to inclusions from 79135 samples, suggested that the recharge will elevate both Ce and H_2O concentrations in the melt and decouple the H_2O/Ce ratio from the source region significantly (Fig. 9A–B), reproducing the compositional evolution trend of all three 79135 inclusions. Much lower MgO concentrations in inclusions hosted by Fo_{71} olivine may reflect the melt entrapment after evacuation from the original reservoir and following magma evolution. If we assumed the melting degree of the source region is 5–30%, as we did for 74220, the required H_2O, S, F, and Cl abundances in the source are 1–4 μg/g, 1–3 μg/g, 0.1–0.8 μg/g, and 0.0003–0.003 μg/g in RFC model (Fig. S10), and 2–13 μg/g, 4–15 μg/g, 0.2–1.8 μg/g, and 0.002–0.02 μg/g in REFC model with 4% mass of evacuation (Table S1 and 2). Likewise, the reduced number of turnovers within the reservoir would increase the aforementioned estimates. For example, with 10

turnovers, the estimated H_2O content of the source becomes 3–23 μg/g and 4–29 μg/g for RFC and REFC models, respectively (Table 2).

Since Su and Zhang (2024) did not report Zr or Ba concentrations of 15597 inclusions after conducting deconvolution to SIMS analysis, we only presented recharge modeling to H_2O/Ce and S/Dy ratios (Fig. 9C–D). If the parental melt of 15597 originated from a primitive cumulate mantle similar to 74220 and 79135, then recharge could still raise the volatile/refractory element ratio as the number of turnovers increases, and the subsequent fractional crystallization causes limited changes to these ratios, resulting in the formation of the inclusions in 15597 with very evolved compositions and elevated volatile/refractory element ratios. Given that subsequent magma evolution without recharge is not expected to fractionate the volatile/refractory element ratios, the mantle source of 15597 melt inclusions must be relatively enriched in S and depleted in H_2O compared to that of the 74220 inclusions (Fig. 9C–D). Considering the calculation above, if the parental melt evolution of the volatile-enriched inclusions is influenced by recharge, then the source region of 79135 inclusions must have similar MgO, S, and F, but lower H_2O and Cl, compared to that of 74220 (Table 2). Therefore, even considering the magmatic recharge process, taking all the melt inclusion data together, it appears that the distribution of volatiles in the primitive lunar mantle is heterogeneous, which may be caused by events such as cumulate mantle overturn (e.g., McCubbin et al., 2015) or the replenishment by the localized late veneers (e.g., Albarède et al., 2015).

7. The evidence of magmatic recharge – future directions

Our study demonstrates how considering magmatic recharge as a pre-entrapment process changes the interpretation of volatile-rich lunar melt inclusions. Magmatic recharge has indeed long been a focus in reconciling the observations of terrestrial magmatic samples. However, the role of continuous melt replenishment in lunar magmatic evolution has not been fully considered. One reason that previous studies did not generally associate lunar volatile-enriched melt with the magmatic recharge process might be that petrological studies did not report zoning in the associated minerals. Take Apollo 74220 inclusion as an example, although the high-pressure multiple saturation point of the melt (~3 GPa; Krawczynski and Grove, 2012) indicates their deep origin, the inclusions were likely captured by their host minerals in shallower magma reservoirs. In this scenario, the host olivine did not experience magmatic recharge process. Additionally, compared to terrestrial basalts, the lower viscosity of lunar mare basalts (e.g., Head and Wilson, 1992; Wilson and Head, 1981) may enhance cation diffusivity, while inhibiting the effectiveness of solute diffusion rate-based mechanisms in forming oscillatory zonation (Elardo and Shearer, 2014; Murase and McBirney, 1970), thereby obscuring the complex zonation associated with recharge. In olivine, Mg and Fe are among the most commonly examined parameters when evaluating compositional zoning (e.g., Elardo and Shearer, 2014; Wong et al., 2025). However, when the temperature of the recharging melt is relatively high (e.g., the primitive 74220 parental magma), diffusion of cations such as Mg and Fe in the host olivine would be further enhanced (Dohmen et al., 2007; Dohmen and Chakraborty, 2007), leading to the homogenization of the elemental distribution. In addition, in the reservoir of the Apollo 74220 affected by magmatic recharge, compatible elements will reach the steady state more rapidly (e.g., ~1 turnovers for Mg; Eq. S6). Once steady state is achieved, even with continuous melt replenishment, the elemental concentrations of the magma and the crystallizing minerals will remain relatively stable and therefore may not produce compositional zoning in the host olivine. Under above circumstances, micro-petrological studies of lunar samples exhibiting textural anomalies are crucial. For terrestrial studies, in addition to reverse zoning, the mineral resorption and subsequent reaction, such as resorbed quartz with a pyroxene jacket found in terrestrial andesite (Eichelberger, 1978), has been treated as a robust index suggesting the replenishment of new melt during the mineral crystallization. Comparable textural features, if identified in lunar samples (e.g., Li et al., 2026), would provide strong independent constraints on recharge processes and should be a focus of future lunar studies.

Another restriction on lunar samples is their limited depth of collection. Some large-scale terrestrial features make it easier to identify the existence of recharge. For instance, the reverse evolution in the composition of lava flow sections of continental flood basalts (e.g., Krans et al., 2024), more evolved compositions at the base transition to more primitive compositions toward the top, as well as upward increases in equilibrium temperatures calculated using mineral thermometers (e.g., Yu et al., 2015), are applied as indicators of magmatic recharge. The cyclic units with mineral reversals, usually the periodic variations of An# in plagioclase and Mg# in olivine and pyroxene (e.g., Brown, 1956; Huppert and Sparks, 1981; Irvine, 1977, Smewing, 1981; Yuan et al., 2017), as well as the homogenous compositions over long distances in cumulate stratigraphy (e.g., Namur et al., 2015; VanTongeren and Mathez, 2013) and abrupt shifts in incompatible trace element ratios (e.g., Zr/Y; Ce/Yb; Djon et al., 2017) observed in the terrestrial layered intrusions, also suggest the occurrence of periodic recharge. Due to the absence of tectonics on the Moon, systematic lithological variations along the profile are difficult to evaluate, but more core sampling by future missions may provide useful information.

Given the limited quantity and sampling locality of the lunar samples mentioned above, examining the geochemical characteristics among samples with the same origin might be the best approach to indicate the role of recharge in the magmatic evolution of the Moon. In mid-ocean ridge basalts, magmatic recharge has been identified through enrichments in incompatible trace elements such as REE, at relatively constant Mg# or FeO* (e.g., O'Hara, 1977; Rannou et al., 2006), a trend that is inconsistent with simple fractional crystallization in a closed system (e.g., O'Neill and Jenner, 2012). Similarly, in continental flood basalts, recharge has been used to explain compatible elements remaining stable or showing increase, while incompatible elements (e.g., K_2O, La, and Nb; Yu et al., 2015) as well as incompatible-element ratios (e.g., Nb/Th, Ce/Pb; Hoyer et al., 2023) increase, which require repeated addition of primitive melts into magma reservoirs.

Finally, magmatic recharge is not only a mechanism for generating compositional anomalies but also an important process for thermally rejuvenating magma reservoirs and extending their lifetimes, as demonstrated in terrestrial systems (e.g., Barboni et al., 2015; Barboni et al., 2016). Remote sensing observations provide a complementary approach, that stratigraphic sequences with multiple lava units of different ages at a single site, such as the multi-stage magmatism with surface age ranging from 3.44 to 2.03 Ga at Chang'e-5 landing site identified by the ejected materials around the crater (Du et al., 2022), may signal the presence of long-lived magma reservoirs that require periodic recharge to sustain prolonged volcanic activity. In summary, applying the above geochemical, petrological, and stratigraphic diagnostics, particularly involving the decoupling between compatible and incompatible elements, to lunar samples represents a promising direction for future work aimed at understanding the dynamics of lunar magmatism.

8. Concluding remarks

Melt inclusions are invaluable samples to probe the interior volatile element chemistry of the Moon. Yet, the chemistry of melt inclusions, particularly the highly incompatible element concentrations and the highly incompatible element to less incompatible element ratios, can be interpreted in more than one way. They can be interpreted utilizing recharge and fractional crystallization from a primitive mantle, or be reproduced via fractional crystallization of melt originating from a relatively more evolved source. Our study provides an alternative explanation to the volatile-enriched nature of some lunar melt inclusions, a signature that results from magmatic recharge rather than a

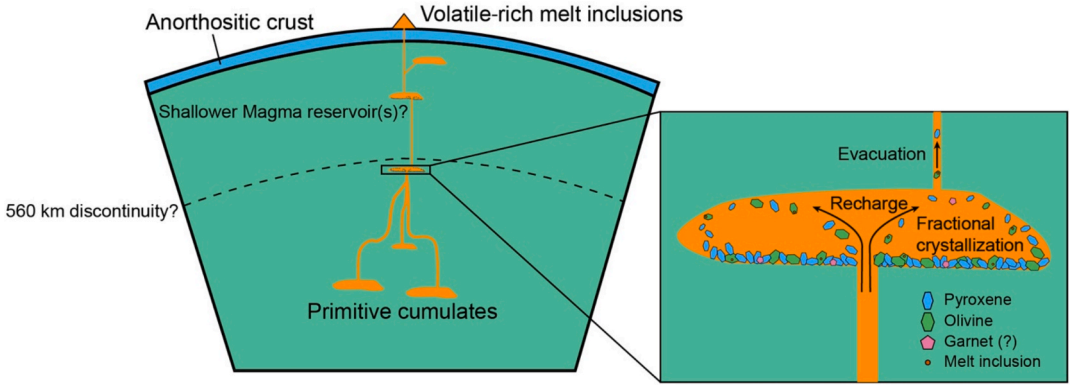

Fig. 10. Schematic illustration showing the scenario for the recharge in the magma reservoir of Apollo 74220 and other volatile-rich, lunar melt inclusions. The parental melt from the deep source region will continuously fill the reservoir and gradually enrich the melt with incompatible elements until reaching a steady state, when concentrations will be buffered by the crystallizing minerals and evacuation, while the major elements could reach the steady state much earlier in the processes (Eqs. S6 and S7). During the recharge process, the melt in the reservoir can be trapped by the crystallizing minerals, forming the melt inclusions with enriched H_2O and Ce concentrations, as well as an H_2O/Ce ratio different from their parental melt.

primary signature representing the source concentration. Melt in the magma reservoir can gradually become enriched in incompatible elements through continuous melt replenishment and fractional crystallization until it approaches the compositional steady state. The major elements reach the steady state in fewer recharge events or cycles compared to the highly incompatible elements. However, as with any modeling, there are caveats. If any melt inclusions experienced post-entrapment degassing that was not corrected for, our estimates of water content may need to be revised slightly upwards. We note, however, that the amount of such degassing is probably small based on previous studies (Ni et al., 2017; Su and Zhang, 2024). We must also acknowledge the uncertainties in our D_{Ce} and D_{H_2O} estimates. In Fig. 2A, we show that H_2O/Ce negatively correlates with D_{H_2O}/D_{Ce}. If D_{H_2O}/D_{Ce} is greater than 1, for example, recharge would actually decrease H_2O/Ce, in which case, we would infer H_2O/Ce ratios and H_2O of the source region to be even higher than values of 74220 inclusions (Fig. S11). Of course, the above recharging effect will be diminished by melt evacuation in the reservoir (Fig. 2B). While uncertainties are large, the Monte-Carlo simulations suggest the D_{H_2O}/D_{Ce} is more likely to be less than 1 (see Supplementary Materials). Based on the above discussions, we argue that magmatic recharge elevates the H_2O/Ce ratios of melt inclusions higher than those in their source regions, even before reaching the compositional steady state. This serves as a cautionary note that, depending on the frequency of the recharge events, recharge can cause the ratios of commonly applied volatile/refractory elements in melt to deviate from the ratios in the source.

Our recharge model suggests the volatile-enriched inclusions from Apollo samples may originate from a highly to moderately volatile-poor

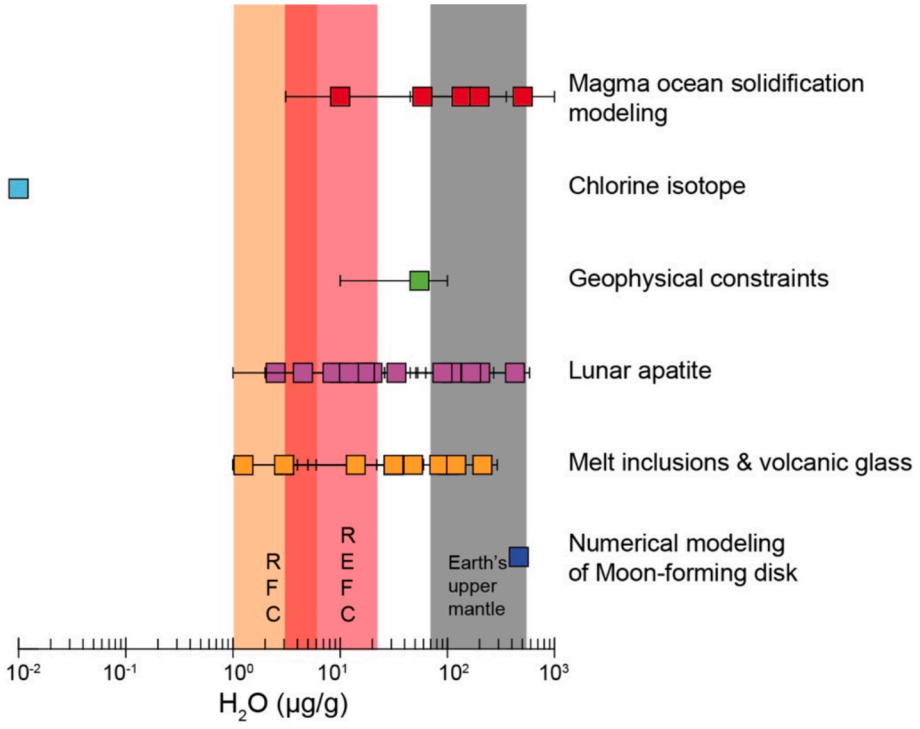

Fig. 11. Estimation of water abundance in the lunar mantle source and estimation methods in corresponding studies. All sources of compiled data are listed in Table S1. The orange and red areas represent the water abundance in the source of Apollo 74220 melt inclusions from this study, estimated by RFC (recharge and fractional crystallization) and REFC (recharge eruption, and fractional crystallization; while eruption ratio is 4 wt%) models, respectively (Tables 1 and 2). The water abundance range of Earth's upper mantle is based on the compilation of water contents in the mantle sources of MORBs listed in Dasgupta and Aubaud (2025).

mantle cumulate (Fig. 10). Considering both the high-temperature and high-pressure multiple saturation point of 74220 orange glass [~1550 °C and 3 GPa; (Green et al., 1975; Krawczynski and Grove, 2012)], and the high MgO and moderately low TiO_2 concentrations (~1.2 wt%; Fig. 8) in the parental melt, the partial melt may be generated from a deep and hybridized mantle cumulate without significant involvement of KREEP (see discussion in Supplementary Materials). The extent of depletion of the incompatible volatile and non-volatile elements in the source compared to literature estimates depends on the efficiency of the magmatic recharge events. More magmatic overturn events yield more depleted source characteristics. The hybridized, volatile-depleted source may have formed and undergone partial melting by gravitationally-driven lunar cumulate mantle overturn (Singletary and Grove, 2008), which could be decoupled from the KREEP component (Su et al., 2022).

To assess the efficiency of the magmatic recharge process during lunar magmatic episodes, further studies are needed regarding complex zonation in lunar minerals and their spatiotemporal correlation with the trace element-enriched samples. Geophysical studies could also shed light on whether complex magma conduit systems may have existed in the lunar interior, thereby providing relevant information on the pathways of magmatic recharge. However, our study suggests that instead of originating from a wet source region, the water-rich lunar melts may derive from water-poor cumulate source regions in the lunar mantle. Our estimated water abundance mantle sources of water-enriched lunar melt inclusions may be up to 1 to 2 orders of magnitude lower than that of the Earth's shallow upper mantle, and lies in the lower end of previous water estimates of the lunar interior (Fig. 11). Even if the magmatic recharge process was not as efficient, considering only a modest number of recharge events leads to significantly lower estimates of volatile elements in the mantle source, consistent with the Moon's volatile depletion relative to the Earth expected from the giant impact origin.

CRediT authorship contribution statement

Dian Ji: Writing – review & editing, Writing – original draft, Investigation, Formal analysis, Data curation, Conceptualization. **Rajdeep Dasgupta:** Writing – review & editing, Supervision, Funding acquisition, Conceptualization. **Cin-Ty Lee:** Writing – review & editing, Supervision, Methodology, Conceptualization.

Data availability

Supporting data are available through Zenodo at https://doi.org/10.5281/zenodo.18111913.

Declaration of competing interest

The authors declare that they have no known competing financial interests or personal relationships that could have appeared to influence the work reported in this paper.

Acknowledgments

We thank Francis Albarède, Nick Dygert, Alberto Saal, Xue Su, Hairuo Fu, Yishen Zhang, and Ye Peng for the helpful discussions. This work benefited from constructive reviews by two anonymous reviewer, and editorial handling by Shichun Huang. This work was supported by NASA grant 80NSSC18K0828. DJ acknowledges a graduate fellowship from the Rice Space Institute Center for Planetary Origins to Habitability (CPO2H).

Appendix A. Supplementary material

Supplementary Materials include three Excel spreadsheets with the supplementary tables, and a PDF file that describes the equations regarding the recharge model, post-entrapment crystallization correction, partition coefficients compilation, discussion on the source of 74220 inclusions, uncertainties and propagation of errors, as well as supplementary figures and tables. Supplementary material to this article can be found online at https://doi.org/10.1016/j.gca.2026.03.042.

References

Albarède, F., 1985. Regime and trace-element evolution of open magma chambers. Nature 318 (6044), 356–358.
Albarède, F., Ballhaus, C., Blichert-Toft, J., Lee, C.-T., Marty, B., Moynier, F., Yin, Q.-Z., 2013. Asteroidal impacts and the origin of terrestrial and lunar volatiles. Icarus 222 (1), 44–52.
Albarède, F., Albalat, E., Lee, C.T.A., 2015. An intrinsic volatility scale relevant to the Earth and Moon and the status of water in the Moon. Meteorit. Planet. Sci. 50 (4), 568–577.
Anderson, A., 1976. Magma mixing: petrological process and volcanological tool. J. Volcanol. Geoth. Res. 1 (1), 3–33.
Astudillo Manosalva, D.F., Elardo, S.M., 2024. Assessing the accuracy of phase equilibrium software in reproducing the liquidus multiple saturation conditions of lunar and Martian basalt compositions. Meteorit. Planet. Sci. 59 (2), 260–285.
Audétat, A., Lowenstern, J.B., 2013. Melt inclusions. In: Treatise on Geochemistry. Second Edition, pp. 143–173.
Barboni, M., Annen, C., Schoene, B., 2015. Evaluating the construction and evolution of upper crustal magma reservoirs with coupled U/Pb zircon geochronology and thermal modeling: a case study from the Mt. Capanne pluton (Elba, Italy). Earth Planet. Sci. Lett. 432, 436–448.
Barboni, M., Boehnke, P., Schmitt, A.K., Harrison, T.M., Shane, P., Bouvier, A.-S., Baumgartner, L., 2016. Warm storage for arc magmas. Proc. Natl. Acad. Sci. 113 (49), 13959–13964.
Barnes, J.J., Tartèse, R., Anand, M., McCubbin, F.M., Franchi, I.A., Starkey, N.A., Russell, S.S., 2014. The origin of water in the primitive Moon as revealed by the lunar highlands samples. Earth Planet. Sci. Lett. 390, 244–252.
Boyce, J.W., Liu, Y., Rossman, G.R., Guan, Y., Eiler, J.M., Stolper, E.M., Taylor, L.A., 2010. Lunar apatite with terrestrial volatile abundances. Nature 466 (7305), 466–469.
Boyd, F.R., Smith, D., 1971. Compositional zoning in pyroxenes from lunar rock 12021, Oceanus Procellarum. J. Petrol. 12 (3), 439–464.
Brown, G.M., 1956. The layered ultrabasic rocks of Rhum, Inner Hebrides. Philos. Trans. Royal Soc. London. Series B, Biol. Sci. 1–53.
Burger, P., Shearer, C., Papike, J., 2009. The multi-stage cooling history of lunar meteorite NWA 032 as recorded by phenocrystic olivine and pyroxene. In: 40th Annual Lunar and Planetary Science Conference, p. 2043.
Cameron, A.G., Ward, W.R., 1976. The origin of the Moon. In: Abstracts of the Lunar and Planetary Science Conference, p. 120.
Canup, R.M., Asphaug, E., 2001. Origin of the Moon in a giant impact near the end of the Earth's formation. Nature 412 (6848), 708–712.
Canup, R.M., Visscher, C., Salmon, J., Fegley Jr, B., 2015. Lunar volatile depletion due to incomplete accretion within an impact-generated disk. Nat. Geosci. 8 (12), 918–921.
Chen, S., Ni, P., Zhang, Y., Gagnon, J., 2022. Trace element partitioning between olivine and melt in lunar basalts. Am. Mineral. 107 (8), 1519–1531.
Chen, Y., Provost, A., Schiano, P., Cluzel, N., 2013. Magma ascent rate and initial water concentration inferred from diffusive water loss from olivine-hosted melt inclusions. Contrib. Miner. Petrol. 165 (3), 525–541.
Chen, Y., Zhang, Y., Liu, Y., Guan, Y., Eiler, J., Stolper, E.M., 2015. Water, fluorine, and sulfur concentrations in the lunar mantle. Earth Planet. Sci. Lett. 427, 37–46.
Chiaradia, M., Müntener, O., Beate, B., 2011. Enriched basaltic andesites from mid-crustal fractional crystallization, recharge, and assimilation (Pilavo Volcano, Western Cordillera of Ecuador). J. Petrol. 52 (6), 1107–1141.
Coogan, L.A., O'Hara, M.J., 2015. MORB differentiation: in situ crystallization in replenished-tapped magma chambers. Geochim. Cosmochim. Acta 158, 147–161.
Crawford, M.L., 1973. Crystallization of plagioclase in mare basalts. In: Proceedings of the Lunar Science Conference, p. 705.
Dasgupta, R., Aubaud, C., 2025. Major volatiles in the Earth's mantle beneath mid-ocean ridges and intraplate ocean islands. Treatise on. Geochemistry 3e 1, 381–423.
Day, J.M., Moynier, F., 2014. Evaporative fractionation of volatile stable isotopes and their bearing on the origin of the Moon. Philos. Trans. R. Soc. A Math. Phys. Eng. Sci. 372 (2024), 20130259.
Day, J.M., Pearson, D.G., Taylor, L.A., 2007. Highly siderophile element constraints on accretion and differentiation of the Earth-Moon system. Science 315 (5809), 217–219.
DePaolo, D.J., 1981. Trace element and isotopic effects of combined wallrock assimilation and fractional crystallization. Earth Planet. Sci. Lett. 53 (2), 189–202.
Ding, S., Hough, T., Dasgupta, R., 2018. New high pressure experiments on sulfide saturation of high-FeO* basalts with variable TiO2 contents–Implications for the sulfur inventory of the lunar interior. Geochim. Cosmochim. Acta 222, 319–339.
Ding, S., Longpré, M.-A., Economos, R., Jackson, Y., Vidal, C.-M., Komorowski, J.-C., Monteleone, B., 2025. Redox and magma recharge controls on excess sulfur build-up at Mount Samalas, 1257 CE. Nat. Commun. 16 (1), 9256.
Dixon, J.E., Leist, L., Langmuir, C., Schilling, J.-G., 2002. Recycled dehydrated lithosphere observed in plume-influenced mid-ocean-ridge basalt. Nature 420 (6914), 385–389.

Djon, L.M., Miller, J.D., Olivo, G.R., Peck, D.C., 2017. Petrogenesis of cyclic units in the northern ultramafic center of the Lac Des Iles complex, Ontario, Canada. Canad. Mineral. 55 (2), 349–374.
Dohmen, R., Becker, H.-W., Chakraborty, S., 2007. Fe–Mg diffusion in olivine I: experimental determination between 700 and 1,200 C as a function of composition, crystal orientation and oxygen fugacity. Phys. Chem. Miner. 34 (6), 389–407.
Dohmen, R., Chakraborty, S., 2007. Fe–Mg diffusion in olivine II: point defect chemistry, change of diffusion mechanisms and a model for calculation of diffusion coefficients in natural olivine. Phys. Chem. Miner. 34 (6), 409–430.
Donaldson, C.H., Brown, R.W., 1977. Refractory megacrysts and magnesium-rich melt inclusions within spinel in oceanic tholeiites: indicators of magma mixing and parental magma composition. Earth Planet. Sci. Lett. 37 (1), 81–89.
Du, J., Fa, W., Gong, S., Liu, Y., Qiao, L., Tai, Y., Zhang, F., Zou, Y., 2022. Thicknesses of mare basalts in the Chang'E-5 landing region: implications for the late-stage volcanism on the moon. J. Geophys. Res. Planets 127 (8), e2022JE007314.
Dygert, N., Liang, Y., Hess, P., 2013. The importance of melt TiO2 in affecting major and trace element partitioning between Fe-Ti oxides and lunar picritic glass melts. Geochim. Cosmochim. Acta 106, 134–151.
Dygert, N., Ji, D., Etheridge, E.N., 2025. A predictive model for divalent element partitioning between clinopyroxene and basaltic melt and an europium-in-plagioclase-clinopyroxene oxybarometer for cumulate rocks. Geochim. Cosmochim. Acta.
Eichelberger, J.C., 1978. Andesitic volcanism and crustal evolution. Nature 275, 21–27.
Elardo, S.M., Shearer Jr., C.K., 2014. Magma chamber dynamics recorded by oscillatory zoning in pyroxene and olivine phenocrysts in basaltic lunar meteorite Northwest Africa 032. Am. Mineral. 99 (2–3), 355–368.
Engels, T., Monteux, J., Boyet, M., Bouhifd, M.A., 2024. Large impacts and their contribution to the water budget of the Early Moon. Icarus 418, 116124.
Fagan, T.J., Kashima, D., Wakabayashi, Y., Suginohara, A., 2014. Case study of magmatic differentiation trends on the Moon based on lunar meteorite Northwest Africa 773 and comparison with Apollo 15 quartz monzodiorite. Geochim. Cosmochim. Acta 133, 97–127.
First, E., Rutherford, M., Welsch, B., 2023. Apollo 17 orange glass magma: olivine reveals complex magmatic history. In: 54th Lunar and Planetary Science Conference, p. 2372.
First, E., Welsch, B., Mitchell, J., Rutherford, M., 2025. Widespread Ti Zoning in Apollo 17 Olivine. In: 56th Lunar and Planetary Science Conference, p. 2873.
Fu, H., Jacobsen, S.B., 2024. Earth-Moon refractory element similarity constrains a thoroughly-mixed Moon-forming disk. Earth Planet. Sci. Lett. 646, 119008.
Gibson Jr, E.K., Andrawes, F., 1978. Sulfur abundances in the 74001/74002 drive tube core from Shorty Crater, Apollo 17. Volume 2.(A79-39176 16-91). In: Lunar and Planetary Science Conference, 9th, Houston, Tex., March 13-17, 1978, Proceedings. Pergamon Press, Inc., New York, pp. 2011–2017.
Ginibre, C., Wörner, G., Kronz, A., 2007. Crystal zoning as an archive for magma evolution. Elements 3 (4), 261–266.
Götze, J., Habermann, D., Kempe, U., Neuser, R.D., Richter, D.K., 1999. Cathodoluminescence microscopy and spectroscopy of plagioclases from lunar soil. Am. Mineral. 84 (7–8), 1027–1032.
Green, D., Ringwood, A., Hibberson, W., Ware, N., 1975. Experimental petrology of Apollo 17 mare basalts. In: Lunar Science Conference, 6th, Houston, Tex., March 17-21, 1975, Proceedings. Pergamon Press, Inc., New York, pp. 871–893. Volume 1. (A78-46603 21-91) Research supported by the California Institute of Technology.
Greenwood, J.P., Itoh, S., Sakamoto, N., Warren, P., Taylor, L., Yurimoto, H., 2011. Hydrogen isotope ratios in lunar rocks indicate delivery of cometary water to the Moon. Nat. Geosci. 4 (2), 79–82.
Hargraves, R., Hollister, L., Otalora, G., 1970. Compositional zoning and its significance in pyroxenes from three coarse-grained lunar samples. Science 167 (3918), 631–633.
Hartmann, W.K., Davis, D.R., 1975. Satellite-sized planetesimals and lunar origin. Icarus 24 (4), 504–515.
Haskin, L., Warren, P., 1991. Lunar chemistry. Lunar Sourcebook 4 (4), 357–474.
Hauri, E.H., Saal, A.E., Rutherford, M.J., Van Orman, J.A., 2015. Water in the Moon's interior: truth and consequences. Earth Planet. Sci. Lett. 409, 252–264.
Hauri, E.H., Weinreich, T., Saal, A.E., Rutherford, M.C., Van Orman, J.A., 2011. High pre-eruptive water contents preserved in lunar melt inclusions. Science 333 (6039), 213–215.
He, H., Li, L., Hu, S., Gao, Y., Gao, L., Zhou, Z., Qiu, M., Zhou, D., Liu, H., Li, R., Hao, J., Hui, H., Lin, Y., 2025. Water abundance in the lunar farside mantle. Nature.
Head III, J.W., Wilson, L., 1992. Lunar mare volcanism: stratigraphy, eruption conditions, and the evolution of secondary crusts. Geochim. Cosmochim. Acta 56 (6), 2155–2175.
Heiken, G., McKay, D., 1974. Petrography of Apollo 17 soils. Proceedings of the Lunar Science Conference, p. 1725. pp. 843–860.
Hess, P.C., Parmentier, E., 1995. A model for the thermal and chemical evolution of the Moon's interior: implications for the onset of mare volcanism. Earth Planet. Sci. Lett. 134 (3–4), 501–514.
Hollister, L., Trzcienski Jr, W., Hargraves, R., Kulick, C., 1971. Petrogenetic significance of pyroxenes in two Apollo 12 samples. In: Proceedings of the Lunar Science Conference, p. 529.
Hoyer, P., Haase, K., Regelous, M., Fluteau, F., 2023. Systematic and temporal geochemical changes in the upper Deccan lavas: implications for the magma plumbing system of flood basalt provinces. Geochem. Geophys. Geosyst. 24 (2), e2022GC010750.
Hu, S., He, H., Ji, J., Lin, Y., Hui, H., Anand, M., Tartèse, R., Yan, Y., Hao, J., Li, R., 2021. A dry lunar mantle reservoir for young mare basalts of Chang'e-5. Nature 600 (7887), 49–53.
Hui, H., Peslier, A.H., Zhang, Y., Neal, C.R., 2013. Water in lunar anorthosites and evidence for a wet early Moon. Nat. Geosci. 6 (3), 177–180.
Huppert, H.E., Sparks, R.S.J., 1981. The fluid dynamics of a basaltic magma chamber replenished by influx of hot, dense ultrabasic magma. Contrib. Miner. Petrol. 75 (3), 279–289.
Husain, L., Schaeffer, O.A., 1973. Lunar volcanism: age of the glass in the Apollo 17 orange soil. Science 180 (4093), 1358–1360.
Irvine, T., 1977. Origin of chromitite layers in the Muskox intrusion and other stratiform intrusions: a new interpretation. Geology 5 (5), 273–277.
Ji, D., Dasgupta, R., 2025. Sulfur inventory of the young lunar mantle constrained by experimental sulfide saturation of Chang'e-5 mare basalts and a new sulfur solubility model for silicate melts in equilibrium with sulfides of variable metal–sulfur ratio. Geochim. Cosmochim. Acta 394, 284–297.
Ji, D., Dygert, N., 2023. Trace element evidence for serial processing of the lunar flotation crust and a depleted bulk Moon. Earth Planet. Sci. Lett. 602, 117958.
Ji, D., Dygert, N., 2024. Trace element partitioning between apatite and silicate melts: effects of major element composition, temperature, and oxygen fugacity, and implications for the volatile element budget of the lunar magma ocean. Geochim. Cosmochim. Acta 369, 141–159.
Kato, C., Moynier, F., Valdes, M.C., Dhaliwal, J.K., Day, J.M., 2015. Extensive volatile loss during formation and differentiation of the Moon. Nat. Commun. 6 (1), 7617.
Krans, S.R., Rooney, T.O., Kappelman, J.W., Yirgu, G., Ayalew, D., 2024. Magma evolution during main-phase continental flood basalt volcanism: a case for recharge-evacuation-assimilation-fractional crystallization in the Ethiopian low-Ti province. Geochem. Geophys. Geosyst. 25 (3), e2023GC011289.
Krawczynski, M.J., Grove, T.L., 2012. Experimental investigation of the influence of oxygen fugacity on the source depths for high titanium lunar ultramafic magmas. Geochim. Cosmochim. Acta 79, 1–19.
Lee, C.-T., Liu, B., 2021. Thick crust, hydrous magmas, and the paradox of voluminous cold magmatism. Volcanica 4 (2), 227–238.
Lee, C.-T., Sun, C., Sharton-Bierig, E., Phelps, P., Borchardt, J., Liu, B., Costin, G., Johnston, A.D., 2022. Widespread phosphorous excess in olivine, rapid crystal growth, and implications for magma dynamics. Volcanica 5 (2), 433–450.
Lee, C.-T.-A., Cheng, X., Horodyskyj, U., 2006. The development and refinement of continental arcs by primary basaltic magmatism, garnet pyroxenite accumulation, basaltic recharge and delamination: insights from the Sierra Nevada, California. Contrib. Miner. Petrol. 151, 222–242.
Lee, C.-T.-A., Lee, T.C., Wu, C.-T., 2014. Modeling the compositional evolution of recharging, evacuating, and fractionating (REFC) magma chambers: implications for differentiation of arc magmas. Geochim. Cosmochim. Acta 143, 8–22.
Li, P.Y., Jiang, Y., Zhao, K., Liao, S.Y., Che, X.C., Zhang, X.R., 2026. . A new pair of lunar gabbroic meteorites record magma recharge at ~ 3.0 Ga. Geochim. Cosmochim. Acta.
Lloyd, A.S., Ruprecht, P., Hauri, E.H., Rose, W., Gonnermann, H.M., Plank, T., 2014. NanoSIMS results from olivine-hosted melt embayments: magma ascent rate during explosive basaltic eruptions. J. Volcanol. Geoth. Res. 283, 1–18.
Lofgren, G.E., Huss, G.R., Wasserburg, G., 2006. An experimental study of trace-element partitioning between Ti-Al-clinopyroxene and melt: equilibrium and kinetic effects including sector zoning. Am. Mineral. 91 (10), 1596–1606.
Lowenstern, J.B., 1995. Applications of silicate-melt inclusions to the study of magmatic volatiles. Magmas, fluids and ore deposits. Mineral. Assoc. Canada Short Course 23, 71–99.
Luo, B., Wang, Z., Song, J., Qian, Y., He, Q., Li, Y., Head, J.W., Moynier, F., Xiao, L., Becker, H., 2023. The magmatic architecture and evolution of the Chang'e-5 lunar basalts. Nat. Geosci. 16 (4), 301–308.
Mallik, A., Schwinger, S., Roy, A., Moitra, P., 2022. Controls on determining the bulk water content of the Moon. Meteorit. Planet. Sci. 57 (12), 2143–2157.
McCubbin, F.M., Vander Kaaden, K.E., Tartèse, R., Klima, R.L., Liu, Y., Mortimer, J., Barnes, J.J., Shearer, C.K., Treiman, A.H., Lawrence, D.J., 2015. Magmatic volatiles (H, C, N, F, S, Cl) in the lunar mantle, crust, and regolith: abundances, distributions, processes, and reservoirs. Am. Mineral. 100 (8–9), 1668–1707.
McIntosh, E.C., Day, J.M., McCubbin, F.M., Vander Kaaden, K.E., Hattingh, R., Porrachia, M., 2024. Revisiting the petrogenesis of pyroclastic glass bead deposits at the Apollo 15 and 17 sites. J. Petrol. 65 (4), egae026.
Michael, P., 1995. Regionally distinctive sources of depleted MORB: evidence from trace elements and H2O. Earth Planet. Sci. Lett. 131 (3–4), 301–320.
Milman-Barris, M.S., Beckett, J.R., Baker, M.B., Hofmann, A.E., Morgan, Z., Crowley, M. R., Vielzeuf, D., Stolper, E., 2008. Zoning of phosphorus in igneous olivine. Contrib. Miner. Petrol. 155 (6), 739–765.
Murase, T., McBirney, A.R., 1970. Viscosity of lunar lavas. Science 167 (3924), 1491–1493.
Namur, O., Abily, B., Boudreau, A.E., Blanchette, F., Bush, J.W., Ceuleneer, G., Charlier, B., Donaldson, C.H., Duchesne, J.-C., Higgins, M.D., 2015. Igneous layering in basaltic magma chambers. In: Layered Intrusions. Springer, pp. 75–152.
Ni, P., Zhang, Y., Chen, S., Gagnon, J., 2019. A melt inclusion study on volatile abundances in the lunar mantle. Geochim. Cosmochim. Acta 249, 17–41.
Ni, P., Zhang, Y., Guan, Y., 2017. Volatile loss during homogenization of lunar melt inclusions. Earth Planet. Sci. Lett. 478, 214–224.
O'Hara, M.J., 1977. Geochemical evolution during fractional crystallisation of a periodically refilled magma chamber. Nature 266 (5602), 503–507.
O'Neill, H.S.C., Jenner, F.E., 2012. The global pattern of trace-element distributions in ocean floor basalts. Nature 491 (7426), 698–704.
Pernet-Fisher, J., Howarth, G., Liu, Y., Chen, Y., Taylor, L., 2014. Estimating the lunar mantle water budget from phosphates: complications associated with silicate-liquid-immiscibility. Geochim. Cosmochim. Acta 144, 326–341.

Portnyagin, M., Mironov, N., Botcharnikov, R., Gurenko, A., Almeev, R.R., Luft, C., Holtz, F., 2019. Dehydration of melt inclusions in olivine and implications for the origin of silica-undersaturated island-arc melts. Earth Planet. Sci. Lett. 517, 95–105.
Potts, N.J., Bromiley, G.D., Brooker, R.A., 2021. An experimental investigation of F, Cl and H2O mineral-melt partitioning in a reduced, model lunar system. Geochim. Cosmochim. Acta 294, 232–254.
Rannou, E., Caroff, M., Cordier, C., 2006. A geochemical approach to model periodically replenished magma chambers: does oscillatory supply account for the magmatic evolution of EPR 17–19°S? Geochim. Cosmochim. Acta 70 (18), 4783–4796.
Rapp, J.F., Draper, D.S., 2018. Fractional crystallization of the lunar magma ocean: updating the dominant paradigm. Meteorit. Planet. Sci. 53, 1452–1455.
Rhodes, J., Dungan, M., Blanchard, D., Long, P., 1979. Magma mixing at mid-ocean ridges: evidence from basalts drilled near 22 N on the Mid-Atlantic Ridge. Tectonophysics 55 (1–2), 35–61.
Ringwood, A., Kesson, S., 1977. Basaltic magmatism and the bulk composition of the moon: II. Siderophile and volatile elements in moon, earth and chondrites: implications for lunar origin. Moon 16 (4), 425–464.
Robinson, K.L., Taylor, G.J., 2014. Heterogeneous distribution of water in the Moon. Nat. Geosci. 7 (6), 401–408.
Rooney, T.O., Krans, S.R., Mège, D., Arnaud, N., Korme, T., Kappelman, J., Yirgu, G., 2018. Constraining the magmatic plumbing system in a zoned continental flood basalt province. Geochem. Geophys. Geosyst. 19 (10), 3917–3944.
Rutherford, M.J., Head, J.W., Saal, A.E., Hauri, E., Wilson, L., 2017. Model for the origin, ascent, and eruption of lunar picritic magmas. Am. Mineral.: J. Earth Planet. Mater. 102 (10), 2045–2053.
Saal, A.E., Hauri, E.H., 2021. Large sulfur isotope fractionation in lunar volcanic glasses reveals the magmatic differentiation and degassing of the Moon. Sci. Adv. 7 (9), eabe4641.
Saal, A.E., Hauri, E.H., Cascio, M.L., Van Orman, J.A., Rutherford, M.C., Cooper, R.F., 2008. Volatile content of lunar volcanic glasses and the presence of water in the Moon's interior. Nature 454 (7201), 192–195.
Saal, A.E., Hauri, E.H., Langmuir, C.H., Perfit, M.R., 2002. Vapour undersaturation in primitive mid-ocean-ridge basalt and the volatile content of Earth's upper mantle. Nature 419 (6906), 451–455.
Saito, K., Alexander, E., 1979. 40AR-39AR studies of lunar soil 74001. In: Lunar And Planetary Science X, P, Abstract, pp. 10491049–10511051.
Sharp, Z., Shearer, C., McKeegan, K., Barnes, J., Wang, Y., 2010. The chlorine isotope composition of the Moon and implications for an anhydrous mantle. Science 329 (5995), 1050–1053.
Shearer, C., Bell, A., Simon, S., Eckley, S., Simon, J., Dottin, J., Wimpenny, J., Gaddis, L., Sharp, Z., Gargano, A., 2024. Combining multi-faceted laboratory studies of 74001-2 and regional remote sensing to address how pyroclastic eruptions record and affect the lunar volatile budget. 55th Lunar and Planetary Science Conference (LPSC). Lunar and Planetary Institute.
Simon, S., Papike, J., Gosselin, D., Laul, J., Hughes, S., Schmitt, R., 1990. Petrology and chemistry of Apollo 17 regolith breccias-A history of mixing of highland and mare regolith. In: Lunar and Planetary Science Conference, 20th, Houston, TX, Mar. 13-17, 1989, Proceedings (A90-33456 14-91). Houston, TX. Lunar and Planetary Institute, pp. 219–230.
Singletary, S., Grove, T., 2008. Origin of lunar high-titanium ultramafic glasses: a hybridized source? Earth Planet. Sci. Lett. 268 (1–2), 182–189.
Smewing, J.D., 1981. Mixing characteristics and compositional differences in mantle-derived melts beneath spreading axes: evidence from cyclically layered rocks in the ophiolite of North Oman. J. Geophys. Res. Solid Earth 86 (B4), 2645–2659.
Srivastava, Y., Basu Sarbadhikari, A., Day, J.M., Yamaguchi, A., Takenouchi, A., 2022. A changing thermal regime revealed from shallow to deep basalt source melting in the Moon. Nat. Commun. 13 (1), 7594.
Srivastava, Y., Basu Sarbadhikari, A., Yamaguchi, A., Takenouchi, A., Day, J., Ubide, T., 2024. Magmatic evolution of KREEP-free lunar meteorite Asuka-881757 inferred from sector-zoned clinopyroxene, pyroxene symplectites, and thermodynamic modeling. Meteorit. Planet. Sci. 59 (11), 2938–2955.
Steenstra, E., Seegers, A., Eising, J., Tomassen, B., Webers, F., Berndt, J., Klemme, S., Matveev, S., van Westrenen, W., 2018. Evidence for a sulfur-undersaturated lunar interior from the solubility of sulfur in lunar melts and sulfide-silicate partitioning of siderophile elements. Geochim. Cosmochim. Acta 231, 130–156.
Steiner, R.A., Rooney, T.O., Girard, G., Rogers, N., Ebinger, C.J., Peterson, L., Phillips, R. K., 2022. Initial Cenozoic magmatic activity in East Africa: new geochemical constraints on magma distribution within the Eocene continental flood basalt province. Geol. Soc. (Lond.) Spec. Publ. 518 (1), 435–465.
Steiner, R.A., Rooney, T.O., Kappelman, J., Lydic, T., Girard, G., Mariita, N., Phillips, R., 2024. Messengers from the magma chambers: petro-stratigraphic analysis of plagioclase-rich flood basalt Lavas in Turkana, Kenya. J. Petrol.
Snyder, G.A., Taylor, L.A., Neal, C.R., 1992. A chemical model for generating the sources of mare basalts: combined equilibrium and fractional crystallization of the lunar magmasphere. Geochim. Cosmochim. Acta 56 (10), 3809–3823.
Stephant, A., Anand, M., Tartèse, R., Zhao, X., Degli-Alessandrini, G., Franchi, I., 2020. The hydrogen isotopic composition of lunar melt inclusions: an interplay of complex magmatic and secondary processes. Geochim. Cosmochim. Acta 284, 196–221.
Streck, M.J., 2008. Mineral textures and zoning as evidence for open system processes. Rev. Mineral. Geochem. 69 (1), 595–622.
Su, B., Yuan, J., Chen, Y., Yang, W., Mitchell, R.N., Hui, H., Wang, H., Tian, H., Li, X.-H., Wu, F.-Y., 2022. Fusible mantle cumulates trigger young mare volcanism on the Cooling Moon. Sci. Adv. 8 (42), eabn2103.
Su, X., Zhang, Y., 2024. Volatiles in melt inclusions from lunar mare basalts: bridging the gap in the H2O/Ce ratio between melt Inclusions in lunar pyroclastic sample 74220 and other mare samples. Geochim. Cosmochim. Acta 373, 232–244.
Tartèse, R., Anand, M., Barnes, J.J., Starkey, N.A., Franchi, I.A., Sano, Y., 2013. The abundance, distribution, and isotopic composition of hydrogen in the Moon as revealed by basaltic lunar samples: implications for the volatile inventory of the Moon. Geochim. Cosmochim. Acta 122, 58–74.
Taylor, S.R., 1982. Planetary Science: A Lunar Perspective. Citeseer.
Taylor, S.R., Taylor, G.J., Taylor, L.A., 2006. The moon: a Taylor perspective. Geochim. Cosmochim. Acta 70 (24), 5904–5918.
Ubide, T., Mollo, S., Zhao, J.-X., Nazzari, M., Scarlato, P., 2019. Sector-zoned clinopyroxene as a recorder of magma history, eruption triggers, and ascent rates. Geochim. Cosmochim. Acta 251, 265–283.
VanTongeren, J., Mathez, E., 2013. Incoming magma composition and style of recharge below the Pyroxenite Marker, Eastern Bushveld complex, South Africa. J. Petrol. 54 (8), 1585–1605.
Walker, D., Shibata, T., DeLong, S.E., 1979. Abyssal tholeiites from the Oceanographer Fracture Zone: II. Phase equilibria and mixing. Contrib. Miner. Petrol. 70 (2), 111–125.
Wallace, P.J., Kamenetsky, V.S., Cervantes, P., 2015. Melt inclusion CO2 contents, pressures of olivine crystallization, and the problem of shrinkage bubbles. Am. Mineral. 100 (4), 787–794.
Wilson, L., Head III, J.W., 1981. Ascent and eruption of basaltic magma on the Earth and Moon. J. Geophys. Res. Solid Earth 86 (B4), 2971–3001.
Wong, K., Morgan, D., Ferguson, D., Edmonds, M., Tadesse, A.Z., Murphy Quinlan, M., Yirgu, G., Wright, T., 2025. Rapid crustal transit of magmas beneath the Main Ethiopian Rift. Nat. Geosci. 1–7.
Xing, C.-M., Wang, C.Y., 2020. Periodic mixing of magmas recorded by oscillatory zoning of the clinopyroxene macrocrysts from an ultrapotassic lamprophyre dyke. J. Petrol. 61 (11–12), egaa103.
Xue, Z., Xiao, L., Neal, C.R., Xu, Y., 2019. Oldest high-Ti basalt and magnesian crustal materials in feldspathic lunar meteorite Dhofar 1428. Geochim. Cosmochim. Acta 266, 74–108.
Yu, X., Chen, L.-H., Zeng, G., 2017. Magmatic recharge buffers the isotopic compositions against crustal contamination in formation of continental flood basalts. Lithos 284, 1–10.
Yu, X., Lee, C.T.A., Chen, L.H., Zeng, G., 2015. Magmatic recharge in continental flood basalts: insights from the C hifeng igneous province in I nner M ongolia. Geochem. Geophys. Geosystems 16 (7), 2082–2096.
Yuan, Q., Namur, O., Fischer, L.A., Roberts, R.J., Lü, X., Charlier, B., 2017. Pulses of plagioclase-laden magmas and stratigraphic evolution in the Upper Zone of the Bushveld complex, South Africa. J. Petrol. 58 (8), 1619–1643.
Zhang, Y., 2020. H2O and other volatiles in the Moon, 50 years and on. ACS Earth Space Chem. 4 (9), 1480–1499.
Zhang, Y., 2024. Review of melt inclusions in lunar rocks: constraints on melt and mantle composition and magmatic processes. Eur. J. Mineral. 36, 123–138.